General Disclaimer

One or more of the Following Statements may affect this Document

- This document has been reproduced from the best copy furnished by the organizational source. It is being released in the interest of making available as much information as possible.

- This document may contain data, which exceeds the sheet parameters. It was furnished in this condition by the organizational source and is the best copy available.

- This document may contain tone-on-tone or color graphs, charts and/or pictures, which have been reproduced in black and white.

- This document is paginated as submitted by the original source.

- Portions of this document are not fully legible due to the historical nature of some of the material. However, it is the best reproduction available from the original submission.

NASA TECHNICAL MEMORANDUM

NASA TM X-72682

NASA TM X- 72682

SUBSCALE, HYDROGEN-BURNING, AIRFRAME-INTEGRATED-SCRAMJET: EXPERIMENTAL AND THEORETICAL EVALUATION OF A WATER COOLED STRUT LEADING EDGE

by

S. Z. Pinckney, R. W. Guy, H. L. Beach, and R. C. Rogers

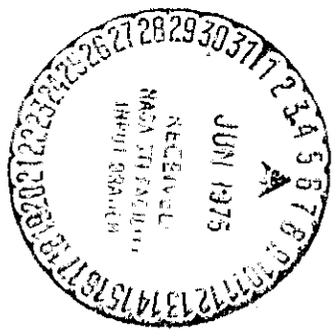

This informal documentation medium is used to provide accelerated or special release of technical information to selected users. The contents may not meet NASA formal editing and publication standards, may be revised, or may be incorporated in another publication.

NATIONAL AERONAUTICS AND SPACE ADMINISTRATION

LANGLEY RESEARCH CENTER, HAMPTON, VIRGINIA 23665

MAY 1975

1. Report No.	2. Government Accession No.	3. Recipient's Catalog No.
NASA TM X-72682		

4. Title and Subtitle	5. Report Date
SUBSCALE, HYDROGEN-BURNING, AIRFRAME-INTEGRATED-SCRAMJET: EXPERIMENTAL AND THEORETICAL EVALUATION OF A WATER COOLED STRUT LEADING EDGE	May 1975
	6. Performing Organization Code

7. Author(s)	8. Performing Organization Report No.
S. Z. Pinckney; R. W. Guy; H. L. Beach; R. C. Rogers	
	10. Work Unit No.

9. Performing Organization Name and Address	11. Contract or Grant No.
NASA Langley Research Center Hampton, VA 23665	
	13. Type of Report and Period Covered
12. Sponsoring Agency Name and Address	Technical Memorandum
National Aeronautics and Space Administration Washington, D.C. 20546	14. Sponsoring Agency Code

15. Supplementary Notes

This is the final release of special information not suitable for formal publication which serves the following need: presents in detail results of a limited investigation for use in other phases of program.

16. Abstract

A water-cooled leading-edge design for an engine/airframe integrated scramjet model strut leading edge has been evaluated experimentally and theoretically. The cooling design employs a copper cooling tube brazed just downstream of the leading edge of a wedge-shaped strut which is constructed of oxygen free copper. The survival of the strut leading edge during a series of tests at stagnation point heating rates ranging from 8.4 to 17.3 MW/m^2 confirms the practicality of the cooling design, and infers that no problem existed either with the low conductivity of the braze material or with voids incurred during the brazing process. In addition, a finite difference thermal model of the strut was proven valid by the reasonable agreement of calculated and measured values of surface temperature and cooling-water heat transfer.

17. Key Words (Suggested by Author(s)) (STAR category underlined)	18. Distribution Statement
Fluid Mechanics and Heat Transfer Leading-edge cooling Scramjet engines Supersonic combustion	Unclassified - Unlimited

19. Security Classif. (of this report)	20. Security Classif. (of this page)	21. No. of Pages	22. Price*
Unclassified	Unclassified	41	$3.75

*Available from { The National Technical Information Service, Springfield, Virginia 22151
STIF/NASA Scientific and Technical Information Facility, P.O. Box 33, College Park, MD 20740

SUBSCALE, HYDROGEN-BURNING, AIRFRAME-INTEGRATED-SCRAMJET: EXPERIMENTAL AND THEORETICAL EVALUATION OF A WATER COOLED STRUT LEADING EDGE

S. L. Pinckney, R. W. Guy, H. L. Beach, and R. C. Rogers

Langley Research Center

SUMMARY

A water-cooled leading-edge for an engine/airframe integrated scramjet model strut leading edge has been evaluated experimentally and theoretically. The cooling design employs a copper cooling tube brazed just downstream of the leading edge of a wedge shaped strut which is constructed of oxygen free copper. The survival of the strut leading edge during a series of tests at stagnation point heating rates ranging from 8.4 to 17.3 MW/m^2 confirms the practicality of the cooling design and infers that no problem existed either with the low conductivity of the braze material or with voids incurred during the brazing process. In addition, a finite difference thermal model of the strut was proven valid by the reasonable agreement of calculated and measured values of surface temperature and cooling-water heat transfer.

INTRODUCTION

Since the beginning of the Hypersonic Ramjet Engine Project (1964), interest in the design and testing of various scramjet engine ideas and models has grown considerably. (See refs. 1-4.) The possibility of high heating rates on engine model sidewall and fuel injector strut leading edges presents the problem of determining if leading edges should be cooled, and how simple the cooling design can be. These problems become particularly evident in relation to a model of the Langley scramjet module (see ref. 5), which is to be tested in a Mach number 7.0 simulated flight enthalpy environment at a flight dynamic pressure of 400 psf. The purpose of this report is to present a theoretical and experimental evaluation of a water-cooled leading-edge strut model designed for use in a high enthalpy supersonic flow. The model is designed to be representative of those to be used in the M = 7.0 engine test.

A variety of techniques exist for constructing engine model strut or sidewall leading edges and their cooling passages; these techniques include drilled cooling passages or the use of a combination of electron beam welding and machining to construct cooling passages. The present investigation considers the brazing of a cooling tube immediately downstream of the leading edge. Two possible problems become evident with this construction technique. These problems are: (1) the low thermal conductivity of the braze material decreases

cooling effectiveness, and (2) any void regions between the tube, braze material, and engine strut or sidewall create hot spots.

The leading-edge cooling model used in the present investigation is a 16.66 degree included angle wedge strut with a 0.76 mm diameter leading edge, which has a 3.2 mm diameter cooling tube brazed within the wedge at 11.7 leading-edge diameters downstream of the strut leading edge. The model was tested in the vitiated heater facility (see ref. 6) in the overexpanded flow of a M = 2.7 nozzle at conditions ranging from 1000° K to 1723° K in stagnation temperature, and from 1.344 MN/m^2 to 2.172 MN/m^2 in stagnation pressure. For each test condition, transient measurements of strut temperature and cooling-water heat-transfer rate are compared with theoretical values predicted using the two-dimensional transient heat-transfer computer program of reference 7.

SYMBOLS

C_f	friction coefficient in a pipe
C_p	specific heat at constant pressure
D	inside diameter of strut cooling tube
h	enthalpy
H	heat-transfer coefficient
p	pressure
Pr	Prandtl number
$\dot{q}$	heat-transfer rate per unit area
T	temperature
T_{av}	average temperature defined by eq. (4)
T_{aw}	surface recovery temperature
T_w	wall temperature at beginning of run
$T_{B,En}$	bulk temperature of cooling water entering the strut
$T_{B,Ex}$	bulk temperature of cooling water leaving the strut
U	velocity
X	distance along surface of strut in direction of flow
α_w	surface angle of the strut relative to flow direction

μ	viscosity
ρ	density

Subscripts:

H_2O	cooling water parameters
stag	stagnation point conditions
t,o	total
w	wall conditions

APPARATUS AND PROCEDURE

Model

The 16.66 degree included angle wedge strut shown in figure 1 is constructed of oxygen free copper. The strut has a 3.2 mm diameter copper cooling tube (cooling water passage is 1.5 mm in diameter) brazed 8.9 mm behind the 0.76 mm diameter leading edge. The cooling water enters the rear of the strut through a 2.3 mm inside diameter tube, passes from the rear of the strut through a drilled hole to the leading-edge cooling tube, and flows through the leading-edge cooling tube to another drilled hole which meets a 2.3 mm inside diameter exit tube. Upstream cooling water pressure was varied from 0.8278 MN/m^2 to 3.499 MN/m^2, while downstream cooling water back pressure was varied from 0.4826 MN/m^2 to 1.55 MN/m^2. Model temperature was measured with a chromel-alumel thermocouple located on the centerline of the wedge 15 mm behind the leading edge and in the spanwise center of the strut. The portion of the inlet and exit cooling water leads and the portion of the chromel-alumel thermocouple lead wire that pass along the back side of the strut, were covered with filler material for thermal protection.

Facility

Experimental tests of the strut model were conducted in the vitiated heater facility described in reference 6. The hot gas of the facility is produced by a hydrogen combustion heater. Hydrogen, oxygen, and air are supplied in such proportions that the resulting vitiated air contains oxygen in a volume fraction equal to that of real air. For these experiments, the operating conditions were from 1.344 MN/m^2 to 2.172 MN/m^2 in stagnation pressure and 1000^o K to 1723^o K in stagnation temperature. The hot gas passes from the combustion heater through a M = 2.7 contoured, two-dimensional nozzle to the atmosphere as a free-jet. A schematic of the M = 2.7 nozzle and the strut is presented in figure 2. The nozzle flow is fully expanded at a heater total pressure of 2.758 MN/m^2; therefore, the nozzle flow is overexpanded for all the present tests and a shock configuration similar to that of figure 2, existed in the nozzle exit flow for all test runs.

Test Procedure

The test procedure consisted of establishing hot flow through the nozzle, inserting the strut model in the hot flow for 5 to 15 seconds, removing the model, and terminating the flow. Experimental data taken consisted of measurements of strut cooling water flow rate using a turbine meter, upstream and downstream strut cooling-water temperatures using copper constantan thermocouples, cooling-water pressures upstream and downstream of the strut, strut temperature, and 16 mm movies of each test to record a failure if it occurred. Hydrogen and air mass flow rates furnished to the vitiated heater were also measure. Using these measurements, the heater fuel-air ratio was calculated and the hot gas stagnation temperatures and other properties were computed using the method of appendix A.

THEORETICAL METHOD

The prediction of the thermal response of materials to a specified environment requires the solution of the governing heat-transfer equations subject to the imposed boundary conditions. The theoretical method and the corresponding computer program used in the present investigation for the solution of the governing transient heat-transfer equations, are given in reference 7. The program can be used for the solution of temperature-time histories for one-dimensional, two-dimensional, and spherical systems. The basic procedure requires that the specific body configuration be divided into a system of small volumes (blocks) and that the size, orientation, material composition, and modes of heat transfer for each individual block and the interrelationships between the blocks be specified. With these inputs the computer program, using an implicit finite difference heat balance method (see ref. 8), solves for the temperatures of the blocks as a function of time. The thermal-balance equations for the individual blocks, the convective heat-transfer options, and the finite-difference algorithm for the solution of the governing equations are also given in reference 7.

The transient heat-transfer computer program requires as input, the local recovery temperature and heat-transfer coefficients (film coefficients) for both the wedge surface and cooling passage walls. The local flow conditions were generated by combining results for the nozzle exit conditions from the combustor design computer program of appendix A, with results for flow conditions behind the shocks from the perfect gas oblique shock tables of reference 9.

A computer program for the stagnation line heat transfer (similar to the method of ref. 10) was used to generate the heat-transfer coefficients at the stagnation line of the strut. Using the stagnation line heat-transfer predictions and an approximate sine relationship,

$$H = \frac{\dot{q}}{T_{aw} - T_w} = \left(\frac{\dot{q}}{T_{aw} - T_w}\right)_{stag} \operatorname{Sin} \alpha_w \qquad (1)$$

the heat-transfer coefficients around the circular part of the strut leading edge were generated. The integral boundary layer computer program of reference 11 was used to generate heat transfer coefficients along the surface of the strut.

The heat-transfer coefficients for the internal surface of the strut leading-edge cooling-water passage were computed using the following standard heat-transfer relationship,

$$\frac{\dot{q}}{T_{aw} - T_w} = \left[\frac{\rho u\, C_p\, C_f}{2\, Pr^{2/3}}\right]_{H_2O} \tag{2}$$

where (see ref. 12, pg. 401, for turbulent flow),

$$C_f = \frac{.3164}{4\left(\frac{\rho u D}{\mu}\right)^{.25}_{H_2O}} \tag{3}$$

In equations (2) and (3) the specific heat "C_p", the Prandtl number "Pr", and the viscosity "μ" of the strut cooling water were computed based on the average temperature given by,

$$T_{av} = \frac{T_w + T_{B,En} + T_{B,Ex}}{3} \tag{4}$$

where "T_w" is the initial strut temperature, and $T_{B,En}$ and $T_{B,Ex}$ are the bulk temperatures of the strut cooling water entering and leaving the strut.

The element model developed to represent the cross section of the strut leading edge and cooling-water passage is shown to scale in figure 3(a) without element identification and in figure 3(b), not to scale, but with the element identification (dimensions in table I). The use of this model to represent the strut assumes that spanwise heat transfer and temperature gradients are negligible, and thus thermal relationships in the strut are two dimensional. The high thermal conductivity of the copper allows great latitude in the choice of block shapes and sizes; therefore, as shown in figure 3, the wedge was somewhat arbitrarily broken up into 55 separate copper blocks, with convection heat transfer along the external surface of the wedge (blocks 1 through 10), convection heat transfer along the internal surface of the cooling-water passage (blocks 11 through 16), and zero convection heat transfer from the rear of the strut and across the wedge centerline. The wetted area of the square section used to represent the cooling-water passage is within 4 percent of that of the actual circular water passage.

RESULTS AND DISCUSSION

Experimental Results

Information pertinent to the seven test runs which were conducted with the strut model, is presented in table II. Included are vitiated heater conditions, cooling-water conditions, local flow conditions behind the nozzle overexpansion shock, and local conditions behind the model bow shock. Also included are values for stagnation line heat transfer and a heat-transfer parameter $\frac{\rho u}{Pr^{2/3}} \frac{h_{t,e} - h_w}{(R/m)^{0.2}}$ which is proportional to the wedge surface heat-transfer rate. The values of these quantities were computed from the local conditions and are used as aids in evaluating data consistency. Since the water flow passage is between the model leading edge and the thermocouple, measured strut temperatures are expected to be more sensitive to the wedge surface heating parameter than to the stagnation line heating rate. Other flow characteristics which affect the measured strut temperature are the boundary layer transition location and the cooling-water flow rate. The heat transfer to the water should be sensitive to both the stagnation line heating and the wedge surface heat transfer.

Plots of measured strut temperature and heat transfer to the cooling water for the various tests are presented as functions of time in figures 4 and 5, respectively. Ordinarily, the strut temperature (see fig. 4) should increase directly with the surface heat-transfer parameter (see table II) and inversely with the cooling-water flow rate. Exceptions to the trend are found in test runs 4 and 5, where run 5 conditions yielded higher strut temperatures with a slightly lower surface heat-transfer parameter and a higher cooling-water flow rate; and in run 6, which has unique characteristics to be discussed later. The higher strut temperatures obtained in test run 5, relative to test run 4, can possibly be attributed to the higher Reynolds number (see table II) which could promote earlier transition in test run 5 and to the higher stagnation heating (see table II) of test run 5.

Comparison of the trends of figure 5 and stagnation line heating ($\dot{q}_{stag}$) from table II shows that heat transfer to the water increases with $\dot{q}_{stag}$. An exception is apparent here also as test run 4 exhibited slightly higher levels of heat transfer to the water than run 3, while $\dot{q}_{stag}$ was nearly the same. However, the surface heating parameter being higher for test run 4 could account for the higher heat transfer to the cooling water.

One effect of cooling-water conditions is evident from a comparison of test runs 5 and 6. Table II indicates that these tests are very similar except for the water flow rate and water pressure level. Figure 4 shows, however, unique behavior for test run 6 when the time exceeded approximately six seconds. Strut temperature rose quite rapidly with a gradient much larger than for any other run. This was indicative of cooling passage boiling, which caused a rapid increase in downstream water pressure (shown by back pressure measurements) and the resultant loss of water flow and cooling effectiveness. Because of the boiling,

heat transfer to the water for test run 6 is not shown on figure 5.

The onset of a failure mode for test run 6 showed that a back pressure of 0.55 MN/m^2 was insufficient to prevent boiling although this same pressure had been adequate for test run 2. For the most severe condition (test run 7), a back pressure of 1.55 MN/m^2 was found to be acceptable to prevent boiling with adequate water flow rate. The survivability of the strut model verifies that the leading-edge fabrication and cooling techniques are sufficient for the conditions tested, and should be more than adequate for the Mach 7 tests.

Theoretical Results

Calculations of temperature distribution through the strut versus time, and heat transfer to the cooling water versus time, were made for the test runs discussed in the previous section. Each set of calculations, except for those of test runs 4 and 7, consisted of predicting the temperature-time histories and cooling-water heat-transfer-time histories, assuming heat-transfer coefficients for all laminar and all turbulent boundary layer flow on the surface of the strut model. The set of theoretical calculations for test runs 4 and 7 also include an additional prediction using heat-transfer coefficients corresponding to laminar boundary layer flow to a point 24.38 mm back of the strut leading edge, followed by a transitional boundary layer region, and then a turbulent boundary layer region over the remainder of the strut. Comparisons of theoretical predictions with experimental data for test runs 4, 7, 5, 1, 2, 3, and 6 are presented in figures 6 through 12, respectively.

The theoretical heat transfer coefficients for test runs 4 and 7 assuming all laminar, all turbulent, and the combination laminar, transitional and turbulent boundary layers on the surface of the strut are presented in figures 6(a) and 7(a). The theoretical and experimental values of the strut temperature versus time, are presented in figures 6(b) and 7(b), and the theoretical and experimental values of the strut cooling-water heat transfer versus time, are presented in figures 6(c), 6(d), 7(c), and 7(d). The two theoretical curves for all turbulent, all laminar and transitional boundary layers given in the latter figures correspond to the minimum and maximum cooling-water passage lengths in the strut. The minimum is the length along the leading edge of the strut, and the maximum includes the passage length through the strut. For cases 4 and 7, the theoretical strut temperature versus time distribution (see figs. 6(b) and 7(b)) using the transitional boundary layer agrees with the experimental strut temperature distribution with reasonable accuracy. The slope of the theoretical temperature versus time curve differs from the experimental data for the first four to five seconds; however, the predicted curves for both tests begin leveling off at about the same value and time as the experimental data. The same trend is seen in the comparison of experimental and theoretical heat transfer to the water in figures 6(d) and 7(d). The choice of block shape and size is believed to be one of the reasons for the difference between the theoretical and experimental results in the early times where the larger gradients occur.

Calculations corresponding to all-turbulent and all-laminar heat transfer on the strut surface predict the upper and lower limits of strut temperature and cooling-water heat transfer. It appears from figures 6(b), 6(d), 7(b), and 7(d) that predicting more reasonable values depends on choosing the correct

transition location. Implicit in this statement is the fact that water-side modeling is sufficiently good. However, the fact that strut temperature and cooling-water heat transfer are coupled would tend to prevent the occurrence of good correlations of both these quantities if the water-side modeling were not sufficient. Since the wetted perimeter of the coolant passage used in the calculations was within 4 percent of the actual case, and reasonable variations of temperature and cooling-water heat transfer (relative to each other) were found, it is concluded that water-side modeling was indeed sufficient for near steady state. Therefore, it can be concluded that predicting the correct equilibrium levels of the strut temperature or cooling-water heat transfer reduces to the problem of predicting the correct transition point. In the present investigation, the assumption for the location of boundary layer transition was checked using the correlation for the transition point recommended in reference 13 for sharp flat plates. This comparison revealed that the assumption of 24.38 mm in the present case landed well within the spread of the experimental data used to obtain the transition point correlation.

Experimental and theoretical results for test runs 5, 1, 2, and 3 are presented in figures 8 through 11. The experimental strut temperatures and cooling-water heat transfers are shown to lie between the two limiting theoretical calculations for all test runs. Since these cases presented no unique problems in analysis beyond those of cases 4 and 7, the transitional calculations were not performed for them.

The experimental and theoretical results of test run 6 are presented in figure 12. As pointed out previously the much larger slope, relative to other test cases, of the experimental strut temperature versus time curve beyond the six second point, is due to cooling water boiling in the strut cooling-water passage, and therefore a reduction in cooling-water passage heat-transfer coefficient. Under these conditions no reliable experimental cooling water heat transfers were obtained for test run 6, and therefore no theoretical values are presented.

The comparisons of experimental and theoretical results (which neglected the braze material) infer that the low conductivity of the braze material has very little effect on cooling effectiveness. This amplifies the earlier conclusion that the braze technique is a viable construction method for strut or engine model sidewall leading edges. As pointed out previously, the upper limit of strut temperature and strut cooling-water heat transfer versus time is predicted using the assumption of all turbulent heat transfer on the strut surface. Therefore, theoretical predictions corresponding to all turublent heat transfer on the strut surface could be used in the conservative design of future configurations. It also appears that judicious selection of the transition location would make design calculations with transition a possibility.

CONCLUDING REMARKS

A water-cooled leading-edge design for a scramjet model strut has been evaluated experimentally and theoretically. The cooling design employs a copper tube brazed just downstream of the leading edge of a wedge shaped strut which

is constructed of oxygen free copper. The experimental and theoretical results infer that the low conductivity of the braze material and any void regions between the strut cooling tube and the strut itself evidently have very little effect on experimental results and thus the braze technique is a possible strut leading edge construction method. Care must be taken, however, to insure not only adequate water flow rates, but water pressures high enough to prevent boiling. An inexpensive transient computational method for thermal analysis in evaluating the cooling necessity of engine model strut and sidewall leading edges was used. Predictions of strut temperature and cooling-water heat transfer versus time, are compared with experimental data obtained by testing the strut model in a vitiated heater facility. Favorable comparison of experimental results and theoretical predictions is a problem of choosing the correct boundary layer transition location. The theoretical upper and lower limits for strut temperature and cooling-water heat transfer versus time were calculated assuming all laminar and all turbulent boundary layer, respectively, on the strut; these values bracket the experimental data. The favorable comparison obtained between experimental and theoretical results demonstrates the successful development of a thermal model for the strut heating and cooling characteristics.

APPENDIX A

A One-Dimensional Computer Program for Supersonic Combustor Design

A computer program for calculating the static pressure and other flow parameter distributions in a one-dimensional supersonic combustor channel has been developed at NASA Langley. Real gas thermodynamic properties for mixtures of hydrogen and air reacted to a specified degree are used for the calculations. Input to the program includes the entering fuel and air states, the channel geometry, and the distribution of fuel injection and fuel reaction with distance along the channel. Output consists of the state at each point calculated along the channel, and line printer plots of selected parameter variations with distance. This computer program is available from Computer Software Management and Information Center, The University of Georgia, Athens, Georgia 30601; under computer program number LAR-11041.

REFERENCES

1. Colley, W. C.; and Harsha, P. T.: Performance Tests of a Supersonic Combustor Having a Wall Step Flameholder. G.E. Rep R65FPD18, April 1965.

2. Kutschenreuter, Paul H., Jr.; et al: Investigation of Hypersonic Inlet Shock-Wave Boundary Layer Interaction. Tech Rep. AFFDL-TR-65-36, G. E. Co., 1965.

3. Billig, F. S.; and Grenleski, S. E.: Direct-Connect and Free-Jet Tests of Scramjet Engine. AIAA Fifth Propulsion Joint Specialist Conf., Colorado Springs, Colorado, S-13, June 1969.

4. Anderson, Griffin Y.; and Gooderum, Paul B.: Explorator Tests of Two Strut Fuel Injectors for Supersonic Combustion. NASA TN D-7581, 1974.

5. Henry, John R.; and Anderson, Griffin, Y.: Design Considerations for the Airframe-Integrated Scramjet. 1st International Symposium on Air Breathing Engines, Marseille, France, June 19-23, 1972.

6. Russin, W. R.: Performance of a Hydrogen Burner to Simulate Air Entering Scramjet Combustors. NASA TN D-7567, February 1974.

7. Garrett, L. B.; and Pitts, J. I.: A General Transient Heat Transfer Computer Program for Thermally Thick Walls. NASA TM X-2058, August 1970.

8. Arpaci, Vedats: Conduction Heat Transfer. Addison-Wesley Pub. Co. C., 1966.

9. Dennard, John S.; and Spencer, Patricia B.: Ideal-Gas Tables for Oblique-Shock Flow Parameters in Air at Mach Numbers from 1.05 to 12.0. NASA TN D-221, March 1964.

10. Bradley, R. G.: Approximate Solutions for Compressible Turbulent Boundary Layer in 3-D Flow. AIAA Jour. vol. 6, no. 5, May 1966.

11. Pinckney, S. Z.: Turbulent Heat Transfer Prediction Method for Application to Scramjet Engines. NASA TN D-7810, September 1974.

12. Schlichting, Dr. Hermann: Boundary Layer Theory. Pergamon Press, New York, New York, 1955.

13. Kuhn, Gary D.: Calculation of Compressible, Nonadiabatic Boundary Layers in Laminar, Transitional and Turbulent Flow by the Method of Integral Relations. NASA CR-1971, November 1971.

TABLE I. - DIMENSIONS OF THERMAL MODEL FOR FIGURE 3

LINE	LENGTH mm	LINE	LENGTH mm
A	0.0399	P	7.64
B	0.251	Q	7.63
C	0 251	R	7.60
D	3.83	S	7.37
E	3.83	T	0.0762
F	1.10	U	0.152
G	0.672	V	0.152
H	1.39	W	0.561
I	10.96	X	0.561
J	7.94	Y	0.177
K	7.93	Z	0.0985
L	7.91	A'	0.023
M	7.89	B'	0.161
N	7.81	C'	7.29
O	7.73		

TABLE II. - EXPERIMENTAL TEST CONDITIONS

		HEATER CONDITIONS			COOLING WATER CONDITIONS			STREAM CONDITIONS IN FRONT OF STRUT			STREAM CONDITIONS ON SURFACE OF STRUT					
TEST #	TUNNEL EXPOSURE TIME, SEC	FUEL / AIR	TOTAL PRESSURE MN/m^2	TOTAL TEMP. ^oK	ENTERING PRESSURE MN/m^2	EXIT PRESSURE MN/m^2	FLOW RATE $m^3/sec \cdot 10^5$	M	ρu kg/m^2sec	$R/m \times 10^7$	M	ρu kg/m^2sec	$R/m \times 10^7$	$\frac{\rho u(h_{t,o} - h_w)}{Pr^{2/3}(R/m)^{.2}} \times 10^7$	$\dot{q}$ stag MW/c^2	Fig. #
1	15	0.008	1.313	1043.9	1.034	0.483	1.915	1.73	946	2.82	1.48	1168	3.24	1.23	8.405	9
2	15	0.01	1.996	1124.6	1.241	0.552	2.540	1.88	1249	3.67	1.60	1555	4.27	5.37	10.372	10
3	15	0.129	2.129	1416.0	2.068	1.069	3.196	2.32	788	2.25	1.97	1012	2.66	5.19	13.087	11
4	15	0.134	1.452	1434.4	2.068	1.069	3.150	1.88	762	1.89	1.61	940	2.18	5.45	12.982	6
5	10	0.136	2.137	1403.4	3.447	1.551	4.670	2.37	819	2.34	2.02	1068	2.80	5.37	13.683	8
6	10	0.15	2.172	1476.7	1.241	0.552	2.660	2.34	767	2.14	2.02	1013	2.57	5.48	13.886	12
7	7.5	0.19	2.172	1702.8	3.447	1.552	4.639	2.40	695	1.73	2.07	922	2.13	6.56	17.309	7

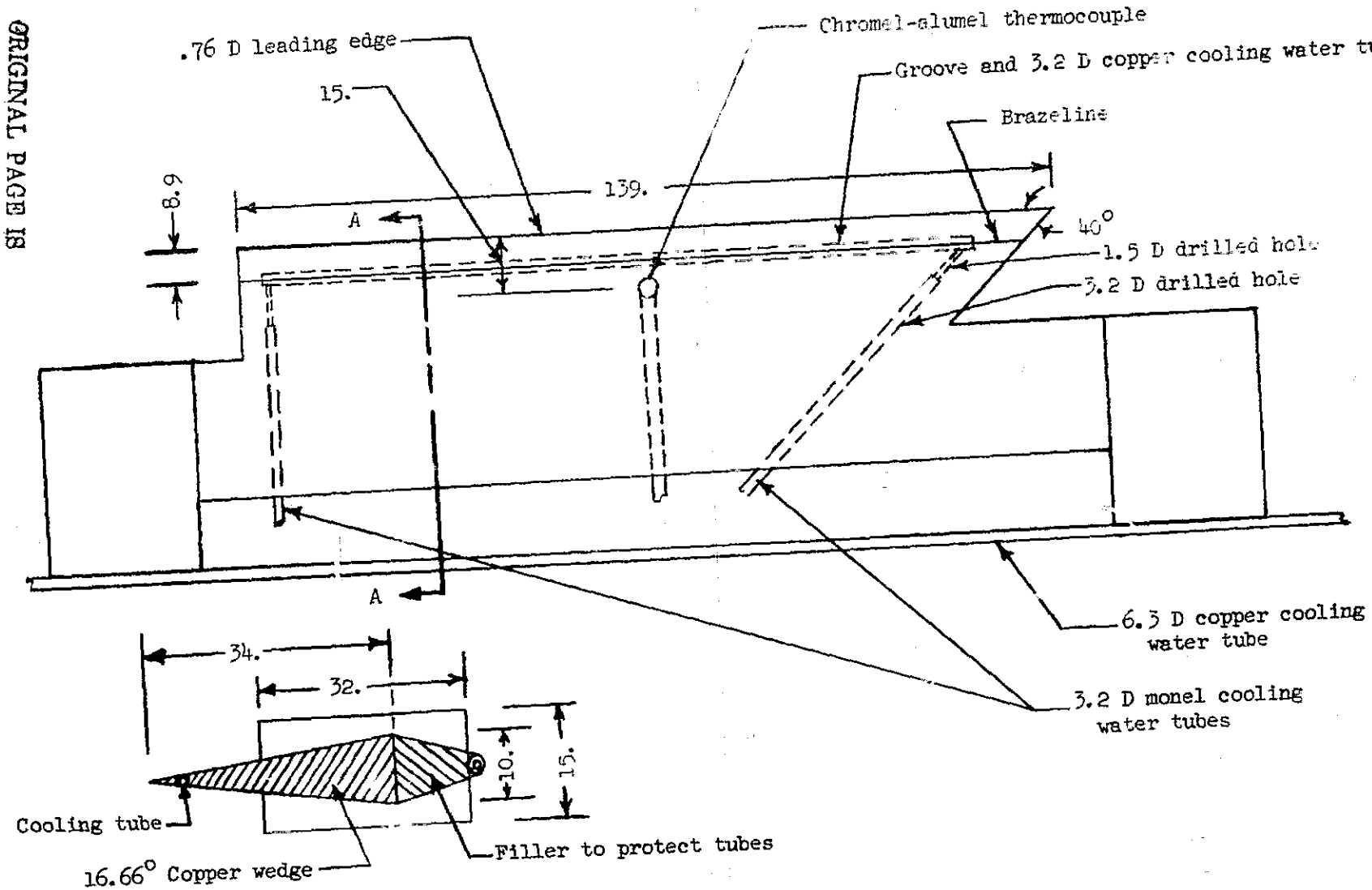

Figure 1. - Strut model. All dimensions are in millimeters.

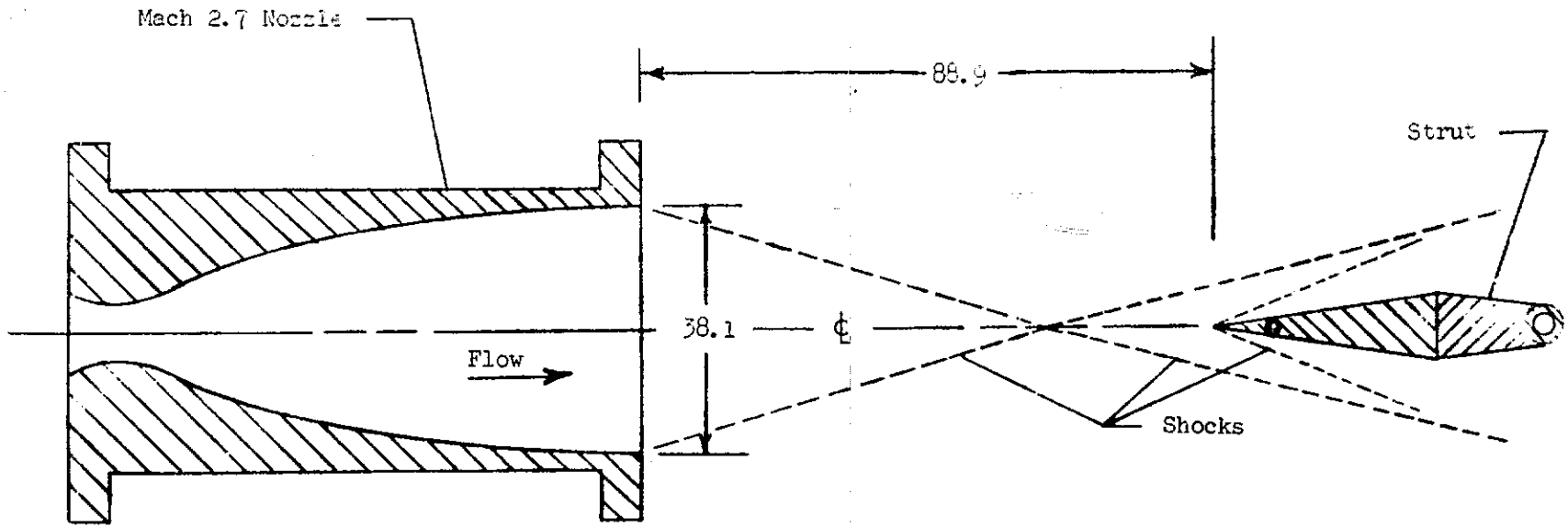

Figure 2. - Mach number 2.7 nozzle with strut in test position. All dimensions are in millimeters.

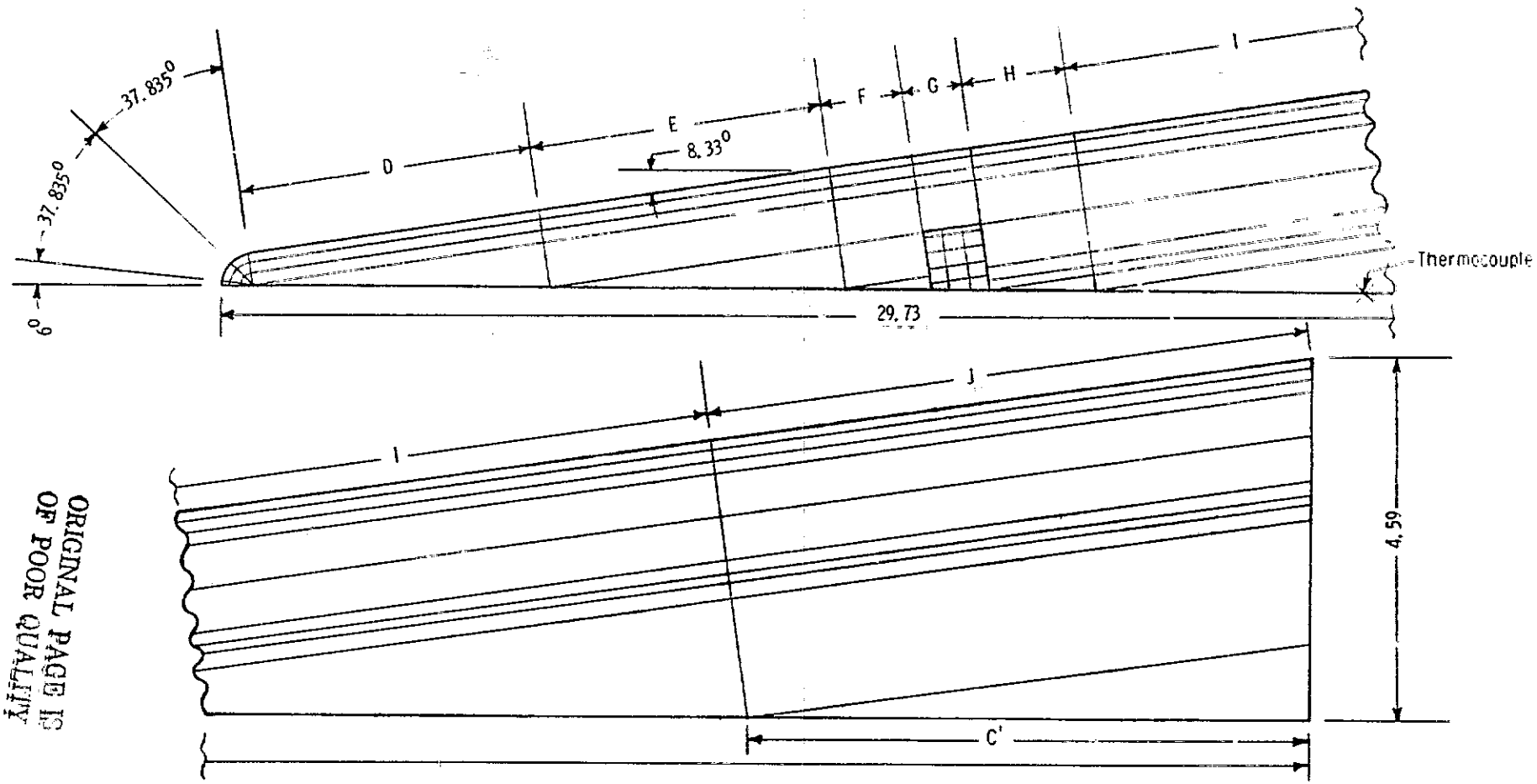

(a) - Element model shown to scale.

Figure 3. - Element modeling of strut cross section used in theoretical calculations. All dimensions are in millimeters. Lengths of A through Z and A' through C' are given in millimeters in Table I.

(b). - Element identification.

Figure 3. — Concluded.

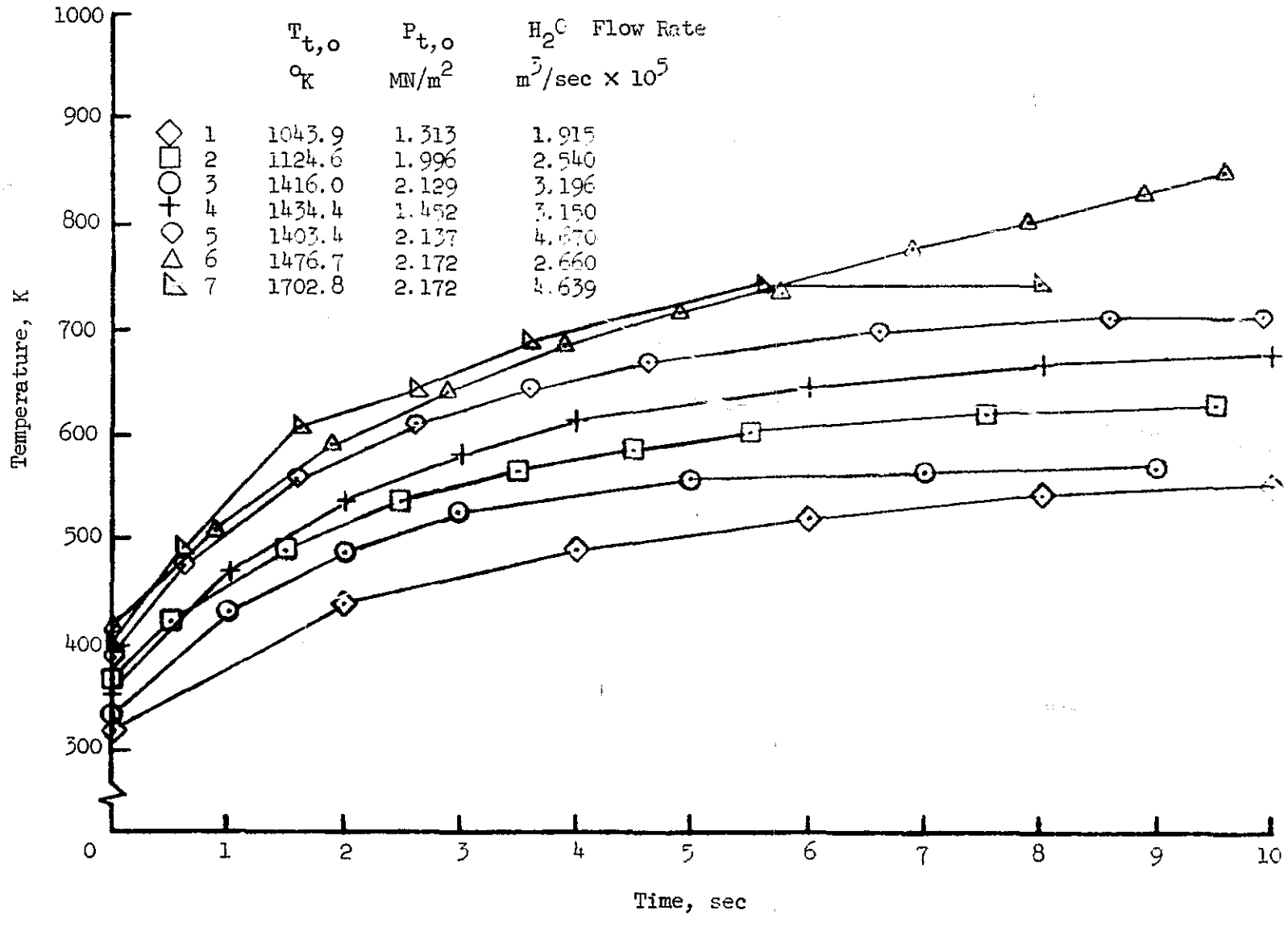

Figure 4. - Measured strut temperature.

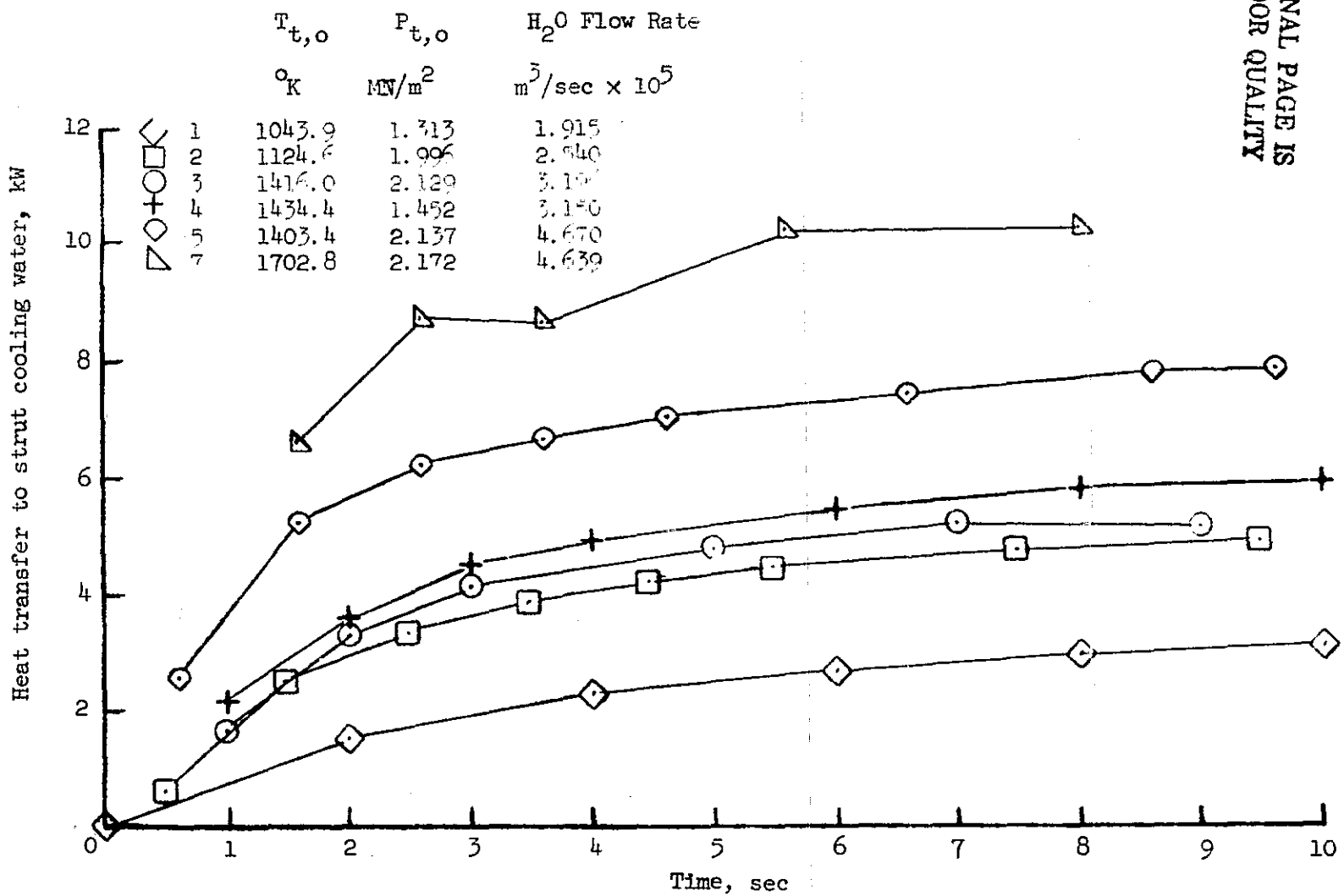

Figure 5. - Measured heat transfer rate to strut cooling water.

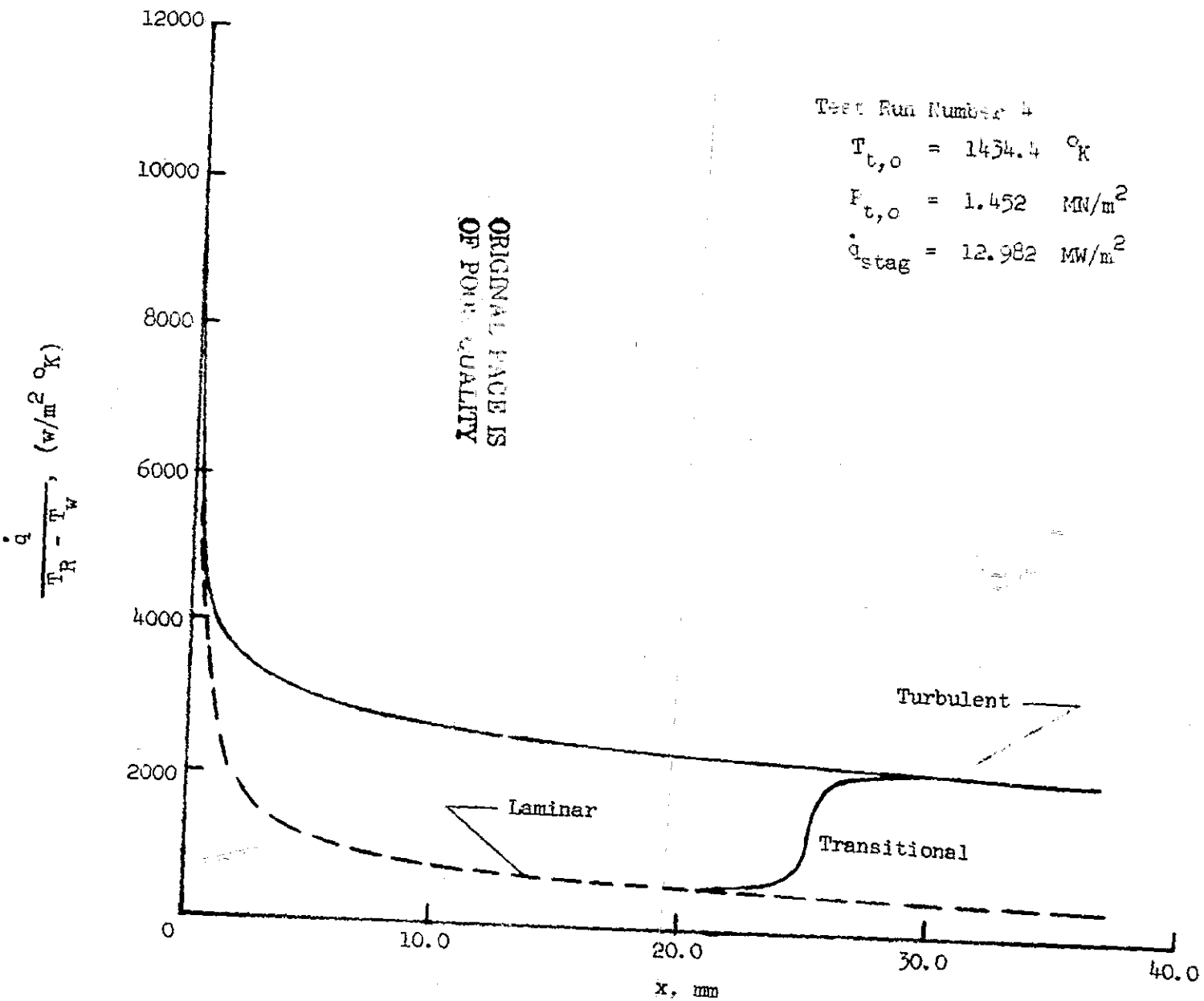

(a) Theoretical heat transfer coefficient al... surface of strut (laminar, turbulent, and transitional boundary layers).

Figure 6. - Experimental data and theoretical results for test run number 4.

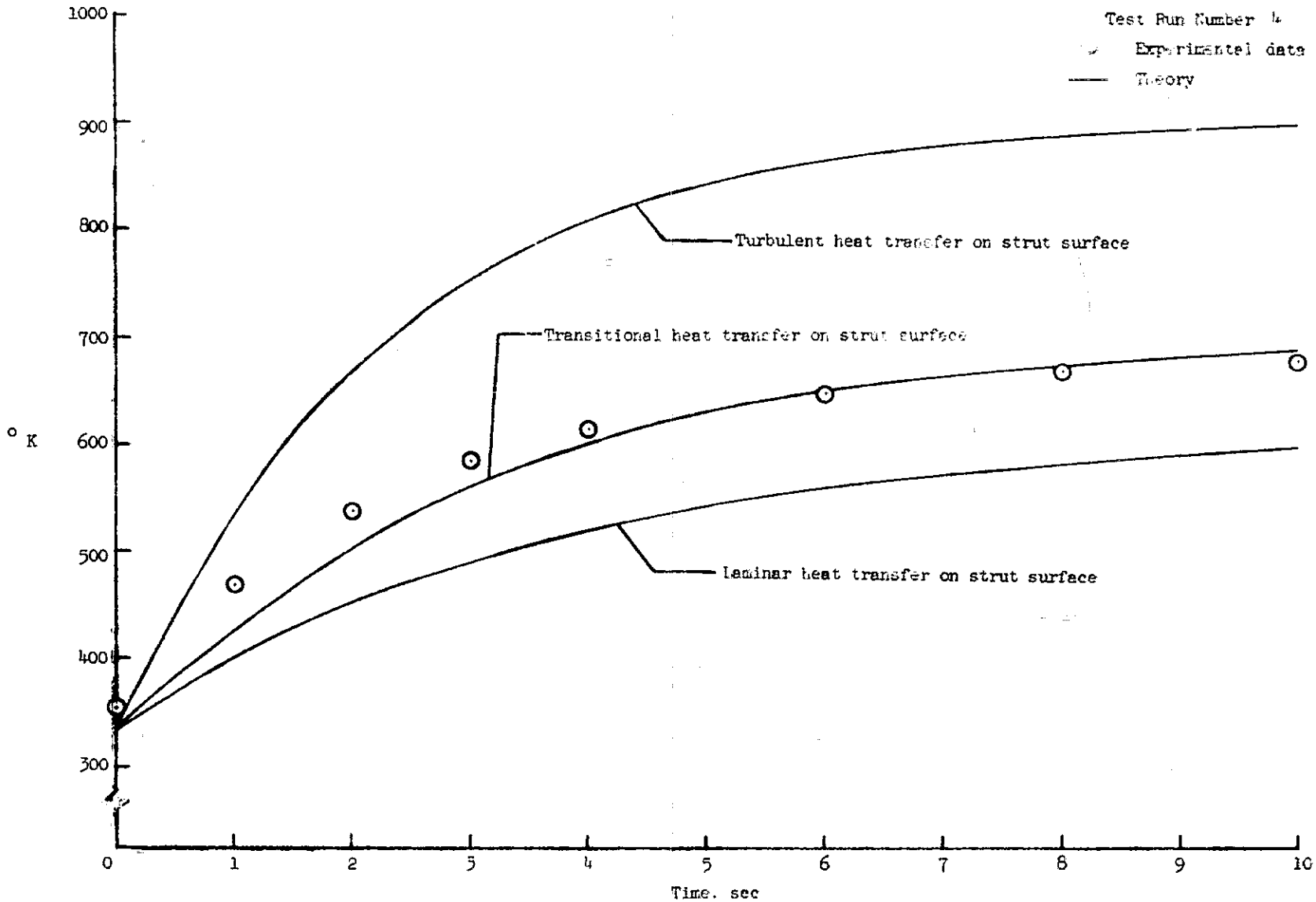

(b) Experimental and theoretical strut temperature versus time (laminar, turbulent, and transitional boundary layers).

Figure 6. - Continued.

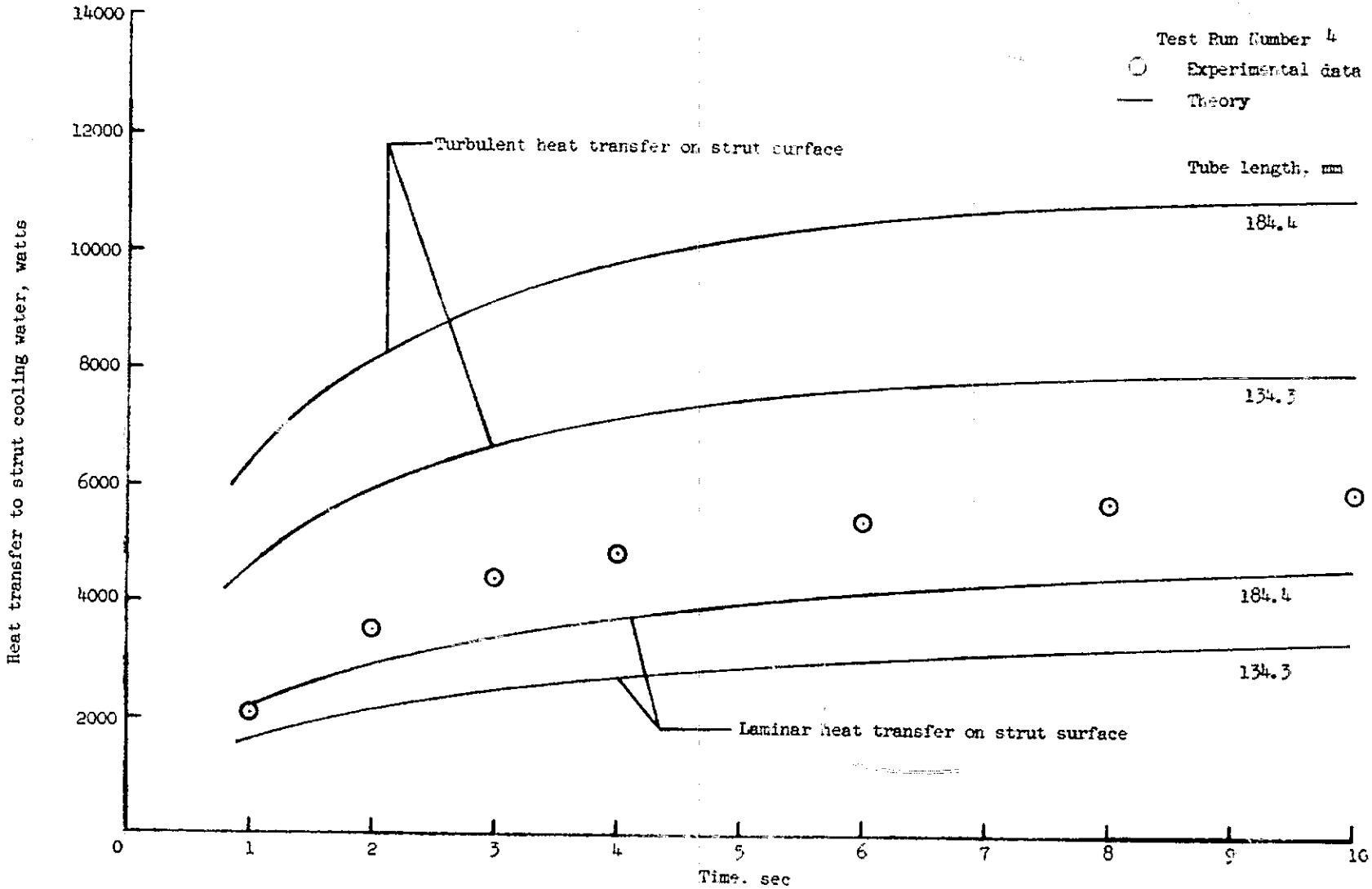

(c) Experimental and theoretical heat transfer rates to strut cooling water versus time (laminar and turbulent boundary layers).

Figure 6.- Continued.

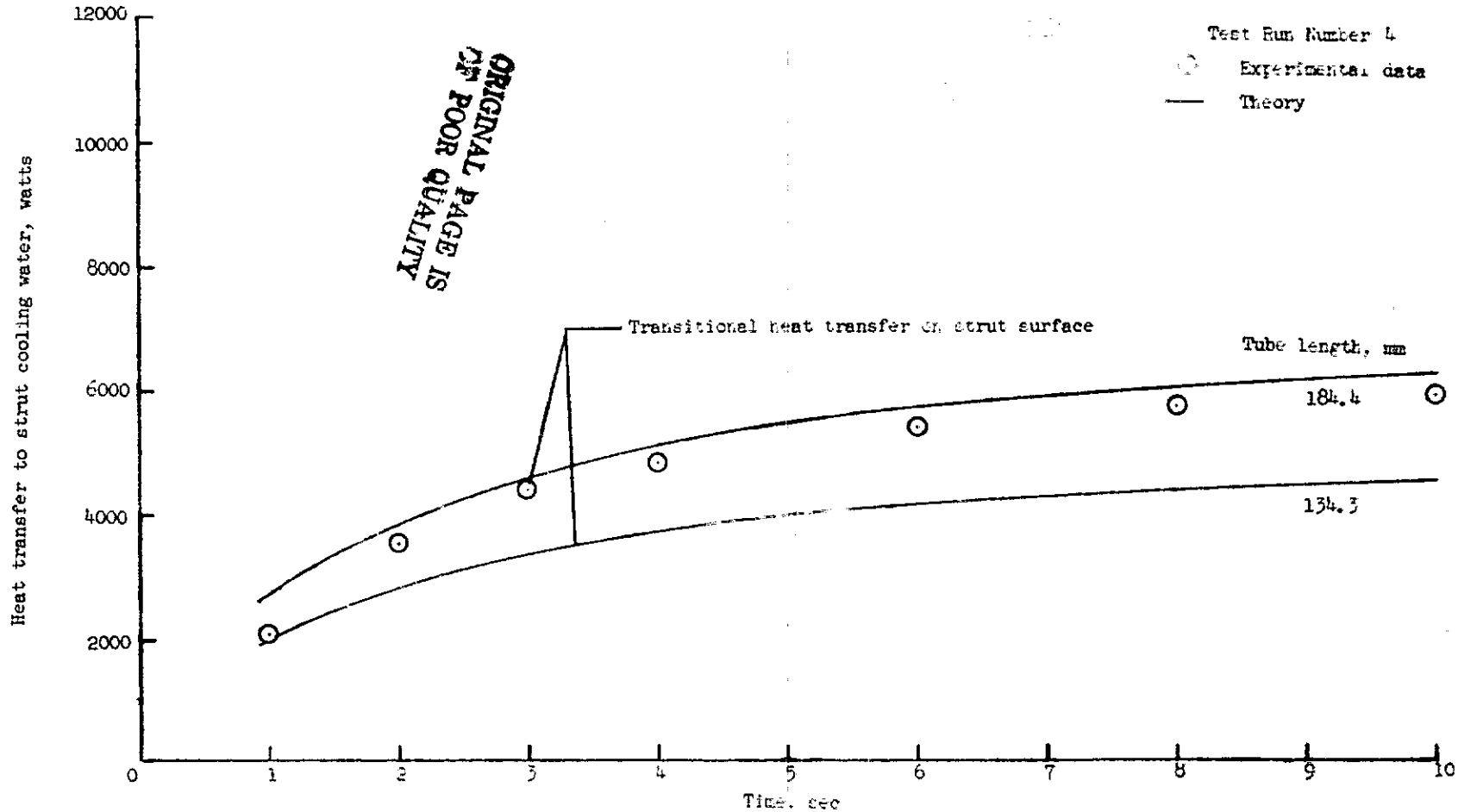

(d) Experimental and theoretical heat transfer rates to strut cooling water versus time (transitional boundary layer).

Figure 6. - Concluded.

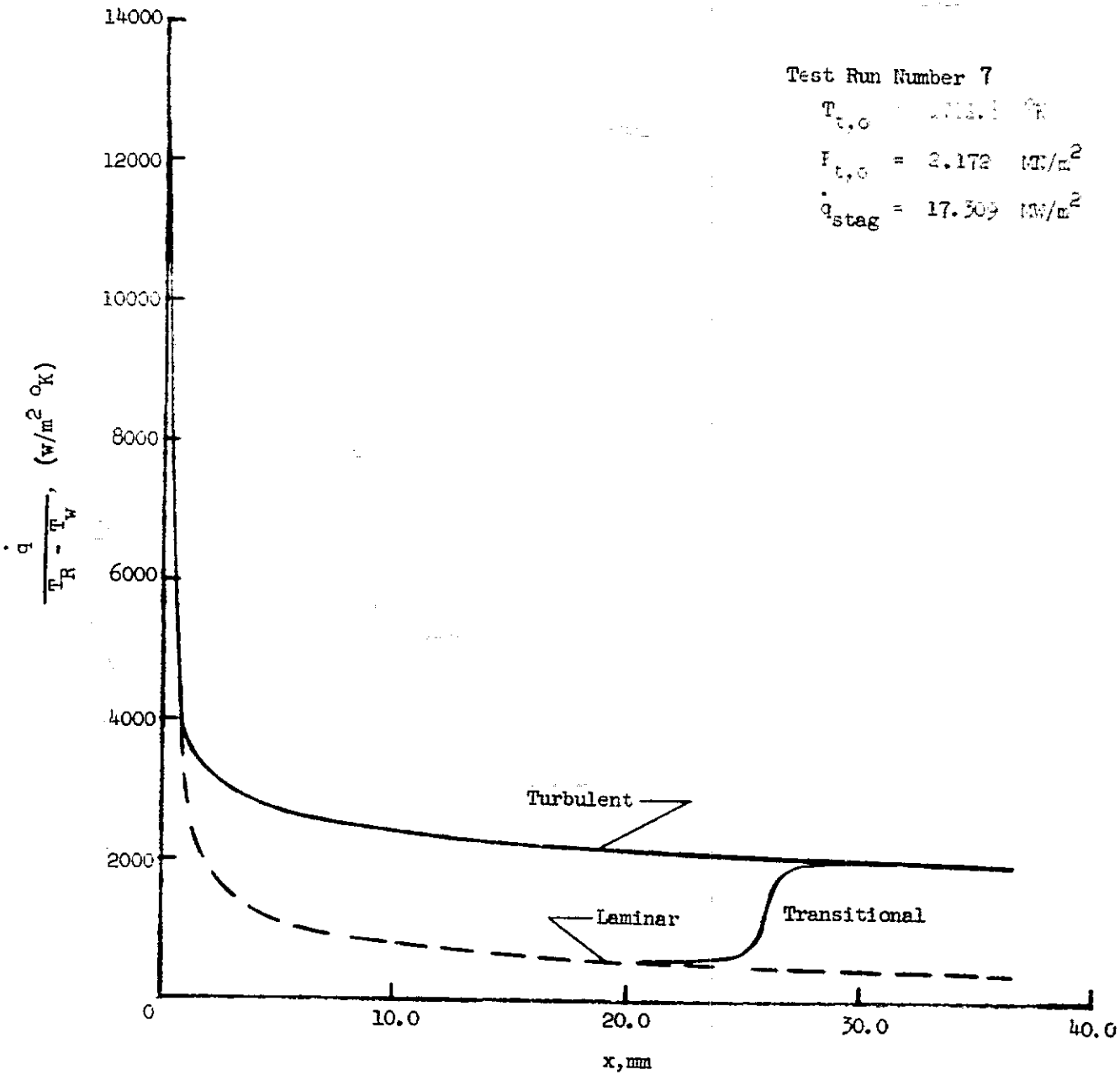

(a) Theoretical heat transfer coefficient along surface of strut (laminar, turbulent, and transitional boundary layers).

Figure 7. - Experimental data and theoretical results for test run number 7.

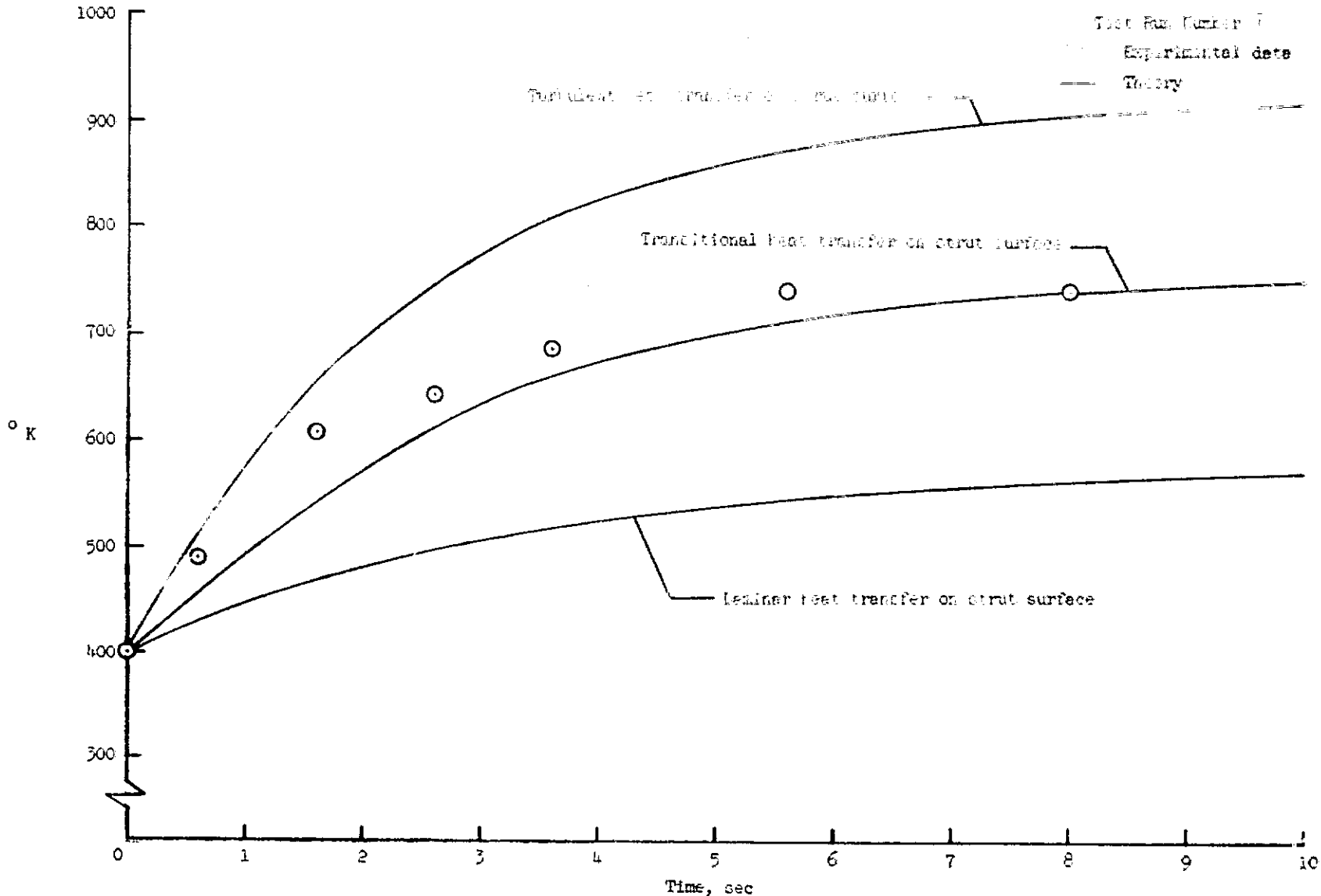

(b) Experimental and theoretical strut temperature versus time (laminar, turbulent, and transitional boundary layers).

Figure 7. - Continued.

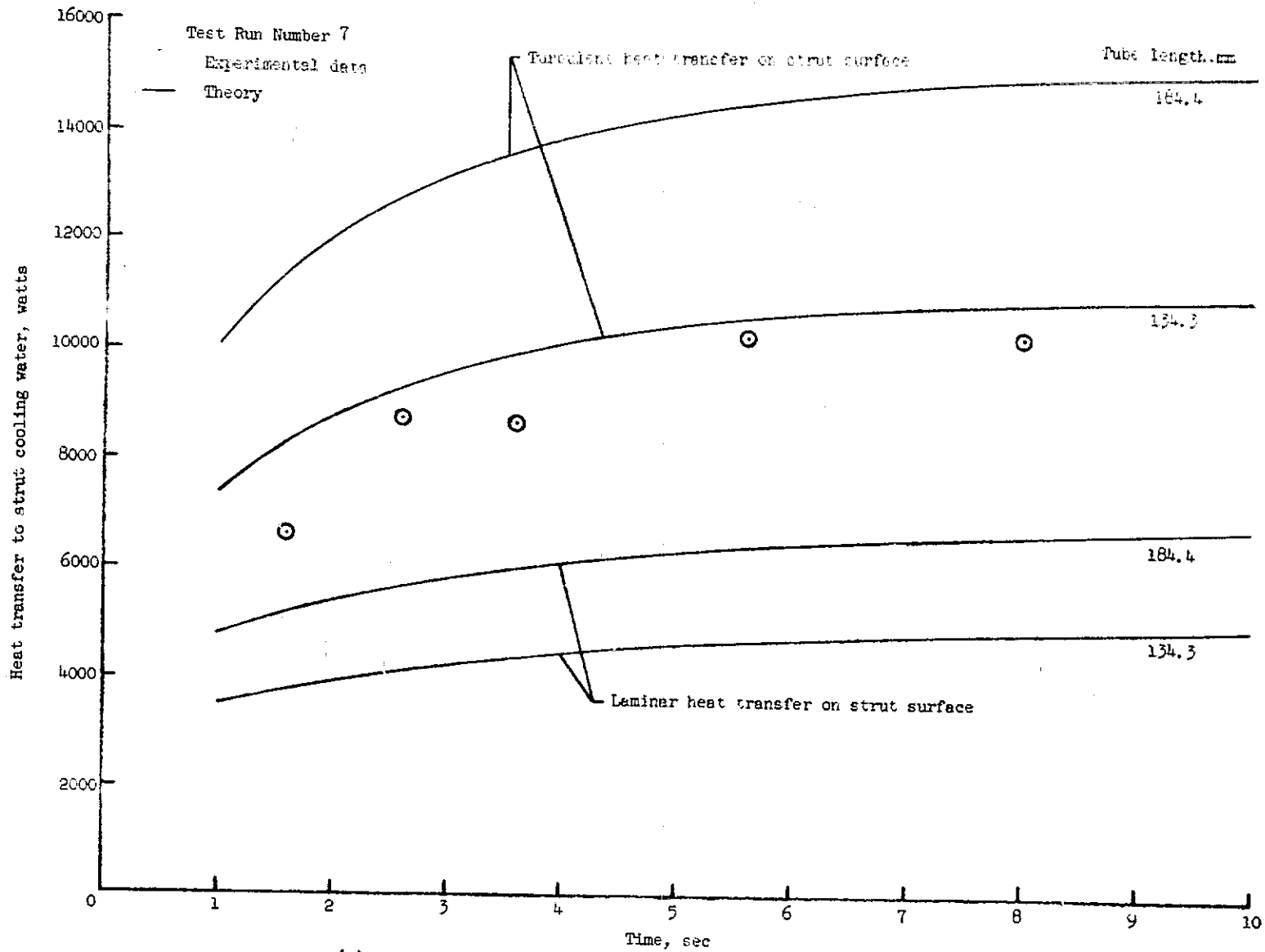

(c) Experimental and theoretical heat transfer rates to strut cooling water versus time (laminar and turbulent boundary layers).

Figure 7. - Continued.

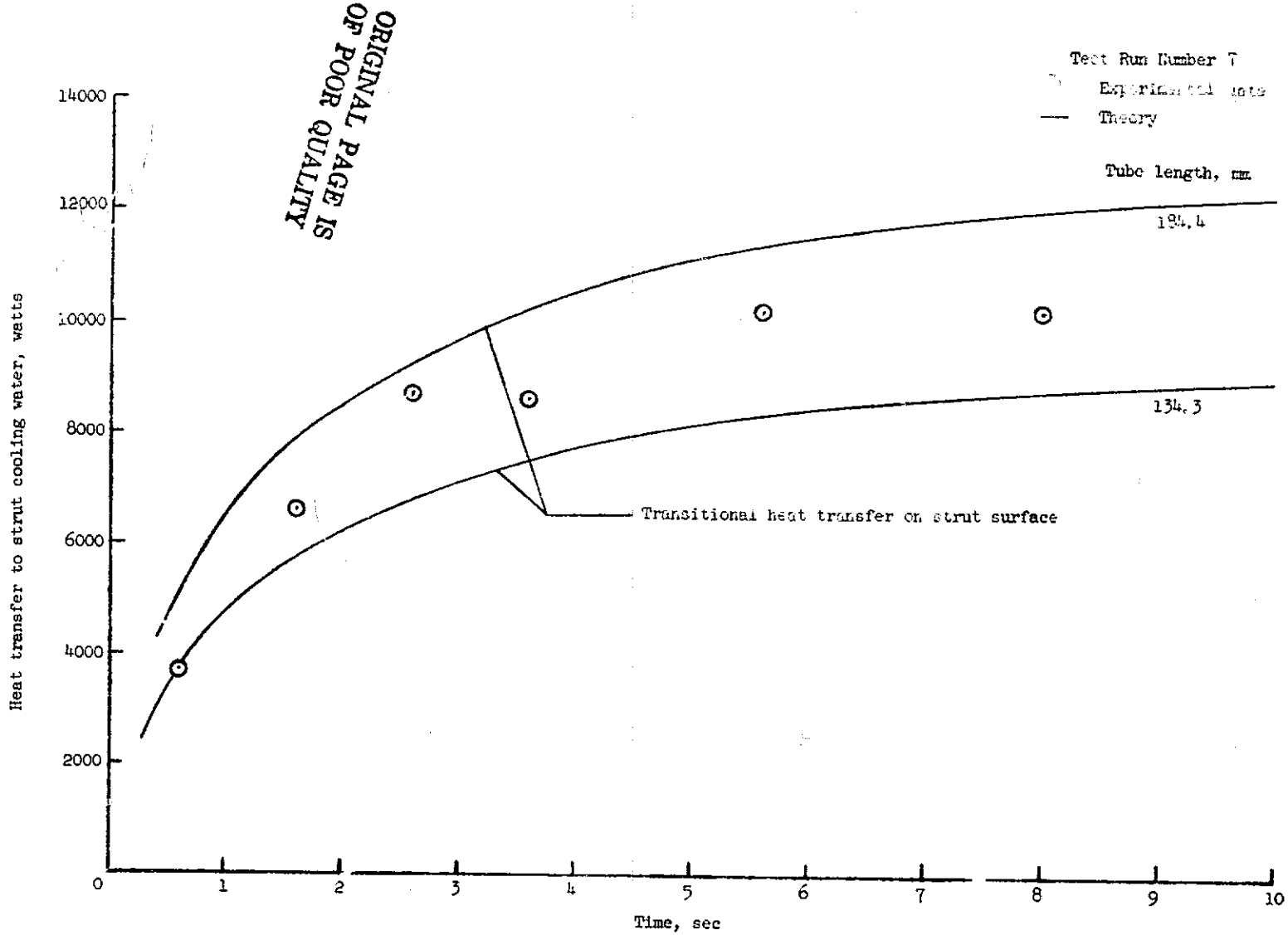

(d) Experimental and theoretical heat transfer rates to strut cooling water versus time (transitional boundary layer).

Figure 7. - Concluded.

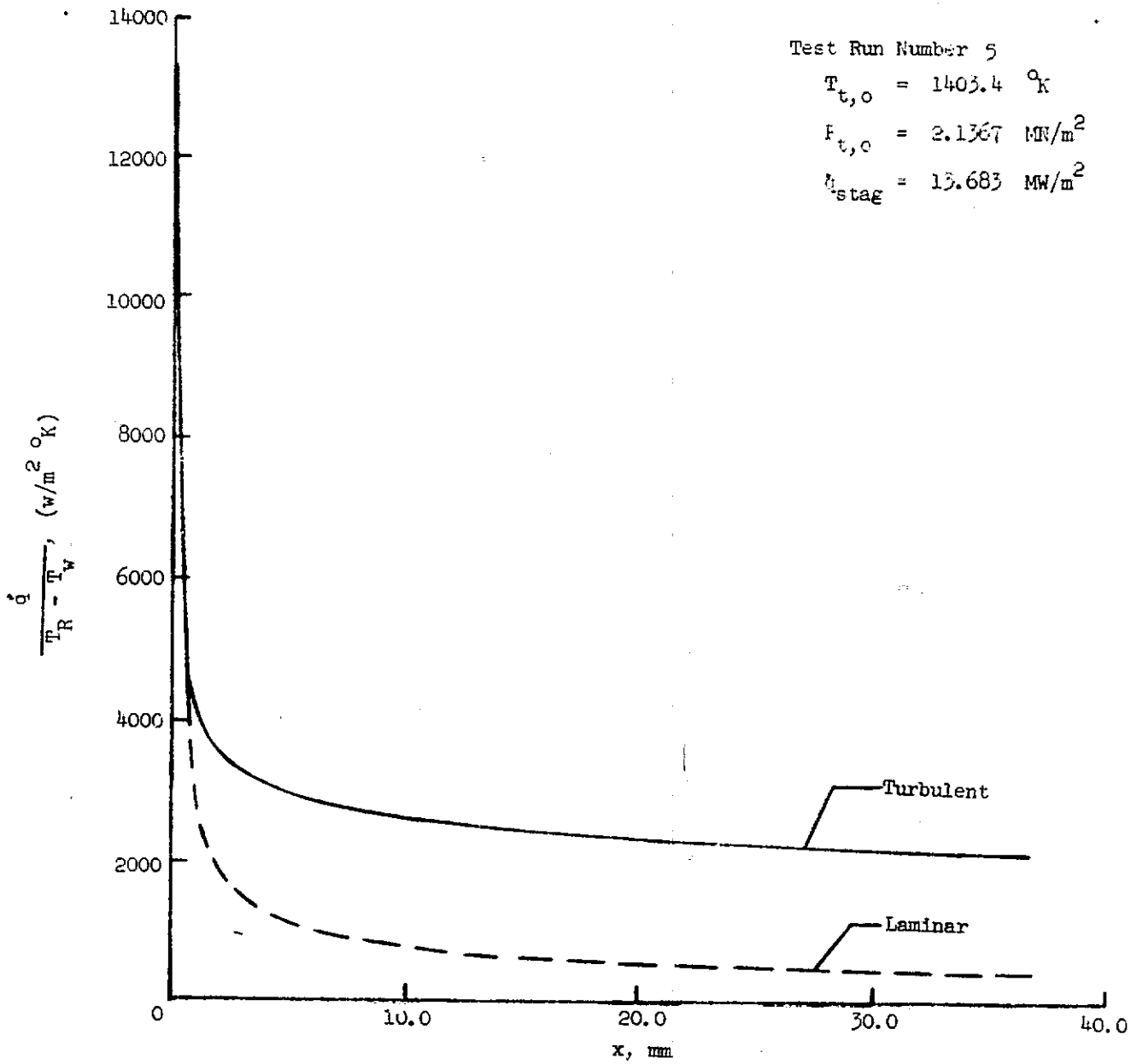

(a) Theorical heat transfer coefficient along surface of strut (laminar and turbulent boundary layers).

Figure 8. - Experimental data and theoretical results for test run number 5.

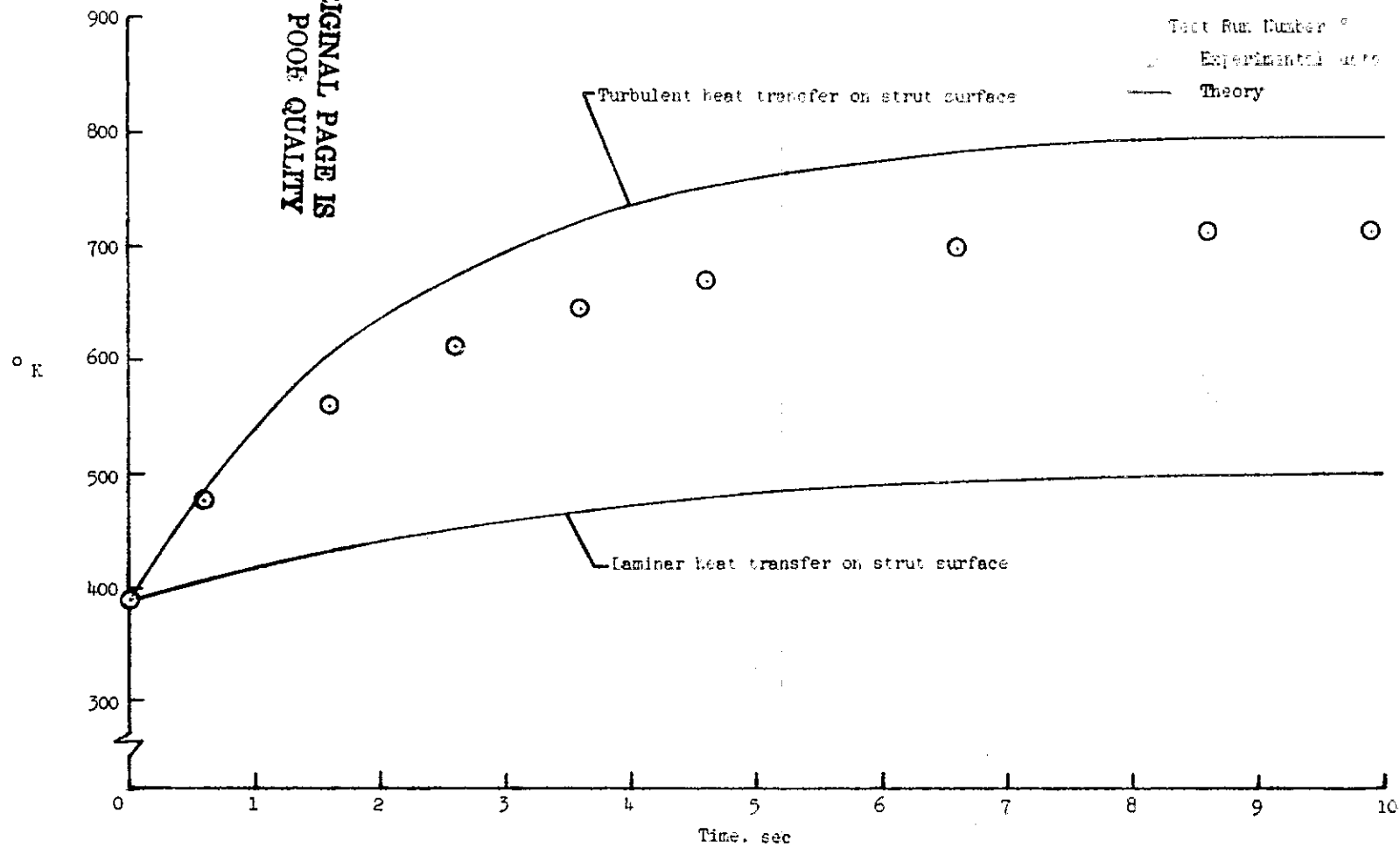

(b) Experimental and theoretical strut temperature versus time (laminar and turbulent boundary layers).

Figure 8. - Continued.

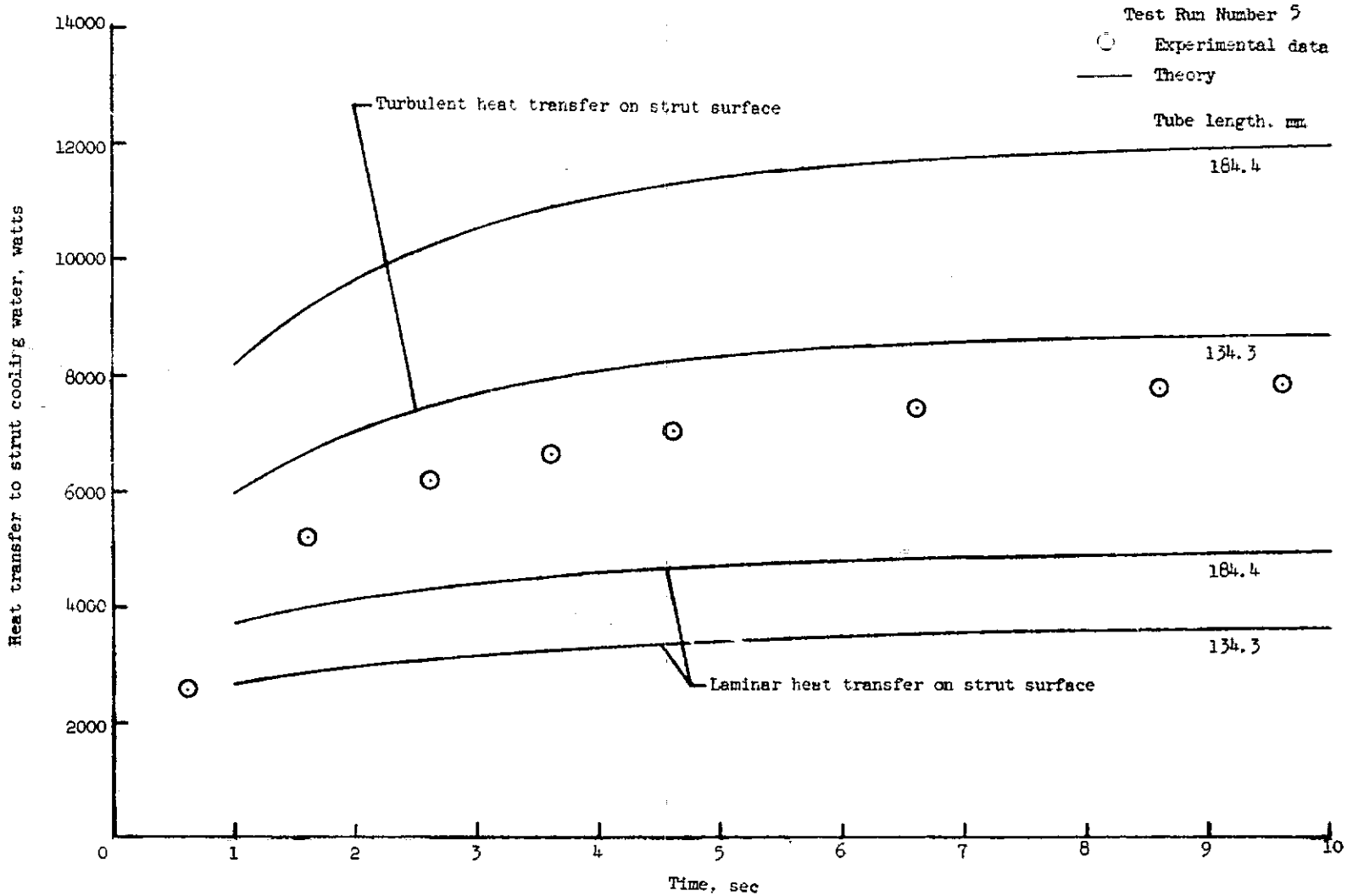

(c) Experimental and theoretical heat transfer rates to strut cooling water versus time (laminar and turbulent boundary layers).

Figure 8. - Concluded.

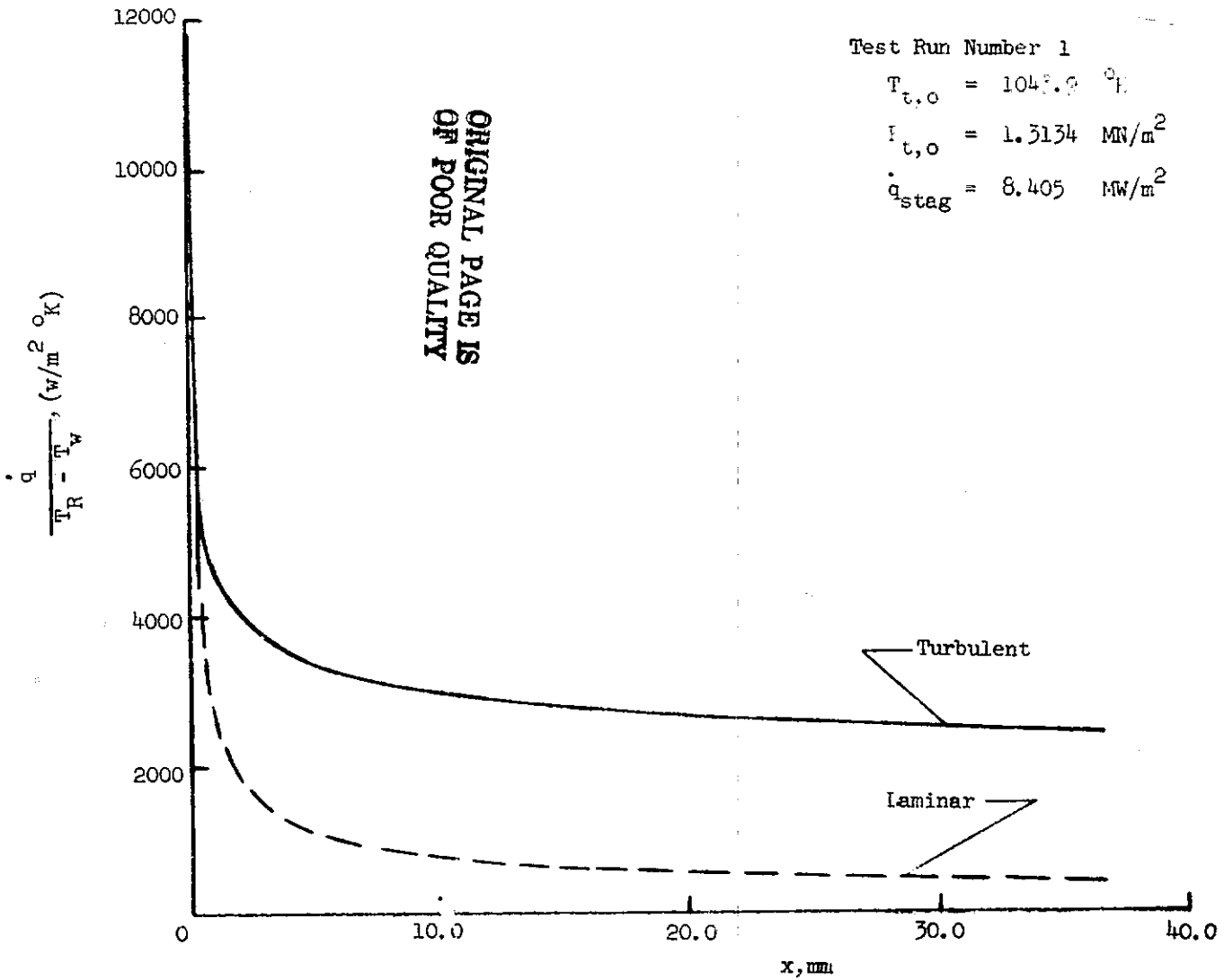

(a) Theoretical heat transfer coefficient along surface of strut (laminar and turbulent boundary layers).

Figure 9. - Experimental data and theoretical results for test run number 1.

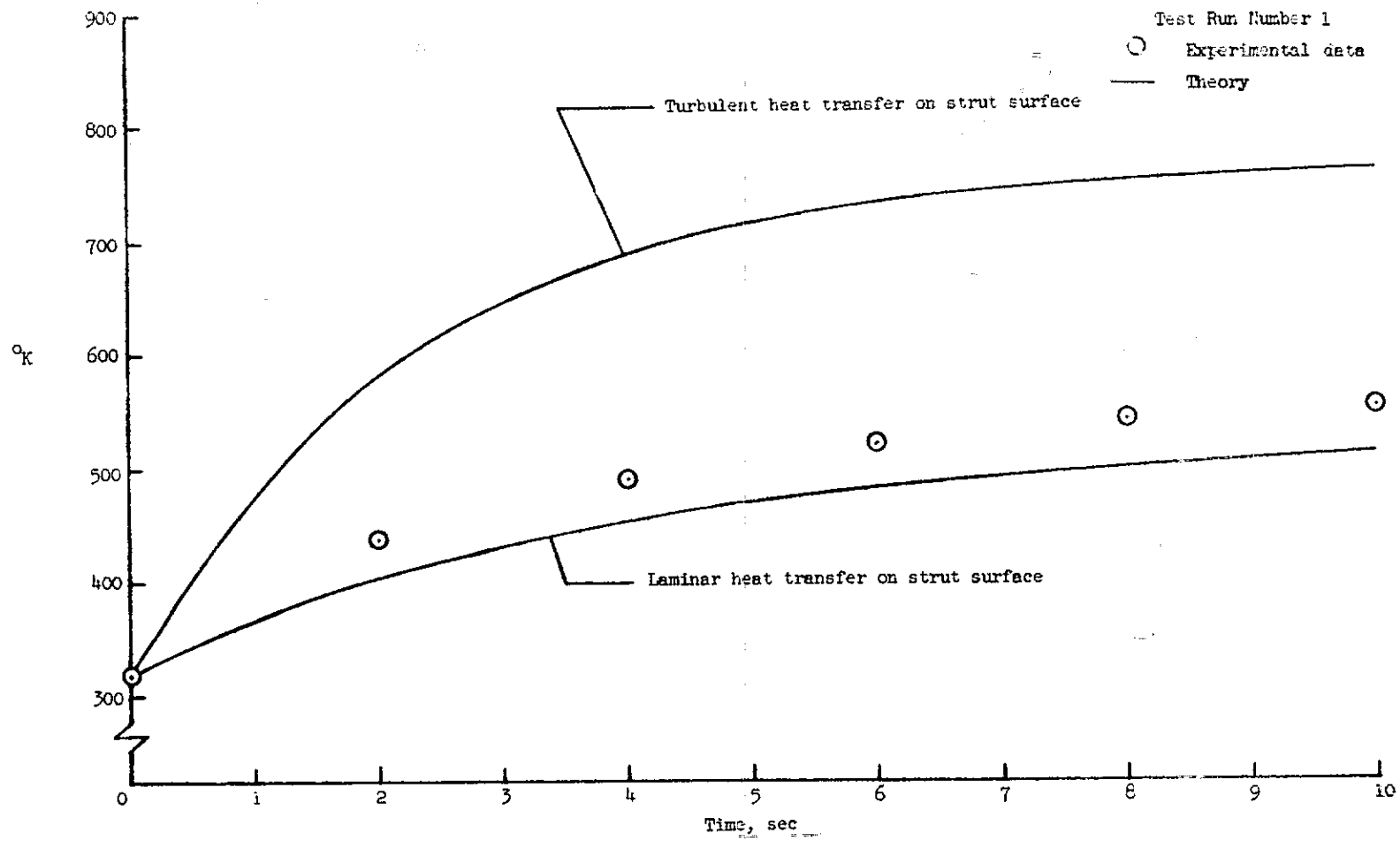

(b) Experimental and theoretical strut temperature versus time (laminar and turbulent boundary layers).

Figure 9. - Continued.

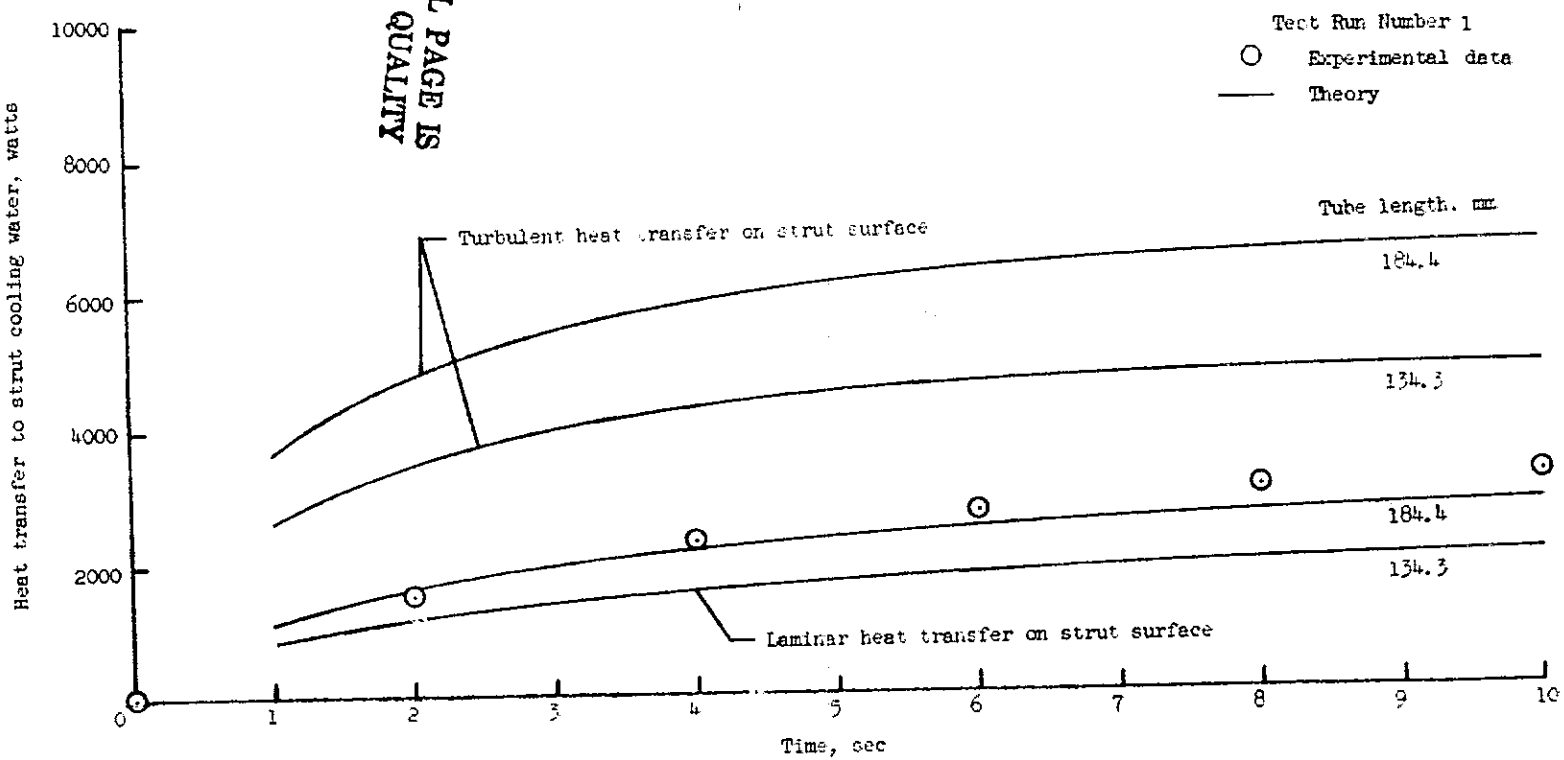

(c) Experimental and theoretical heat transfer rates to strut cooling water versus time (laminar and turbulent boundary layers).

Figure 9. - Concluded.

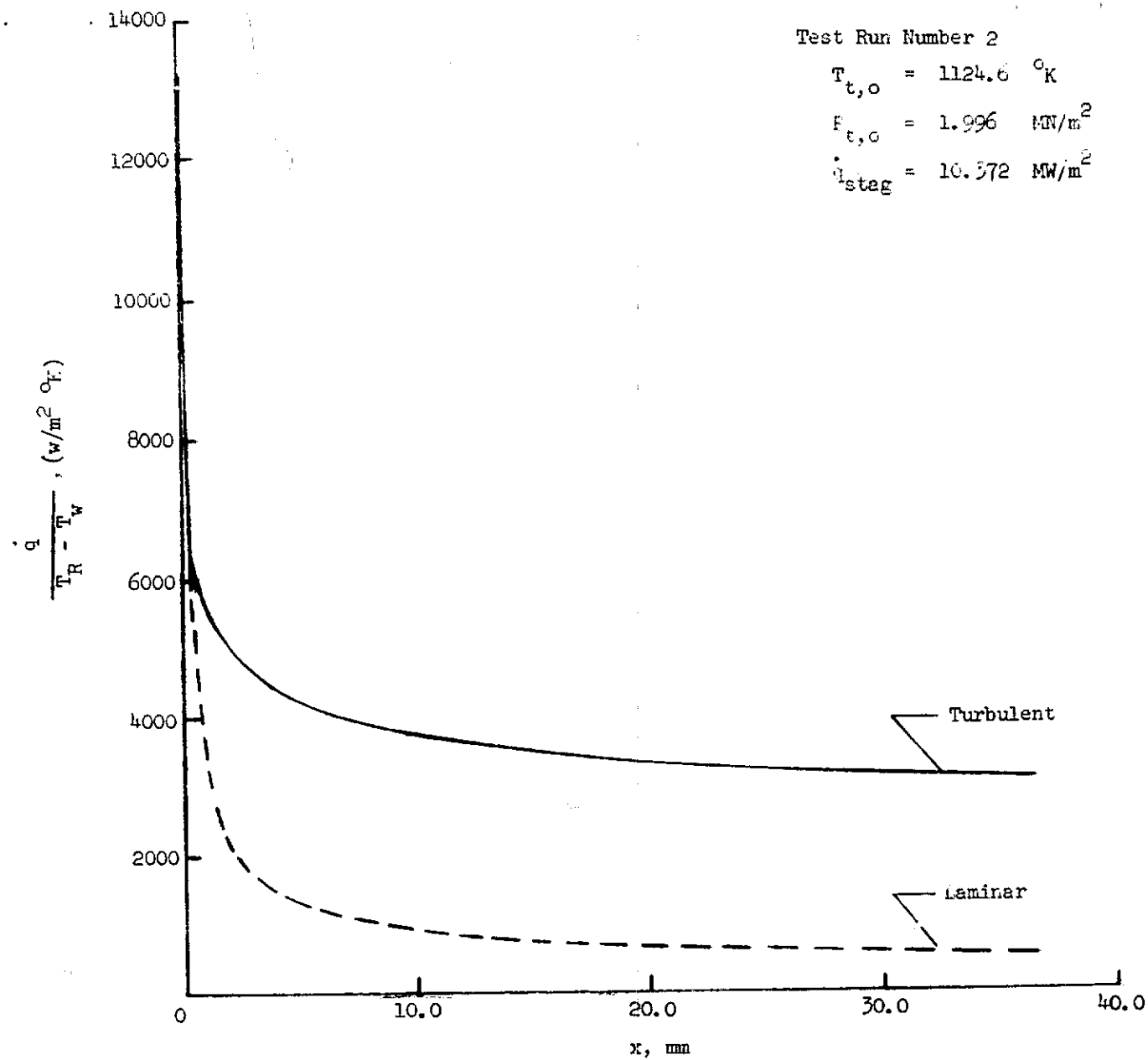

(a) Theoretical heat transfer coefficient along surface of strut (laminar and turbulent boundary layers).

Figure 10. - Experimental data and theoretical results for test run number 2.

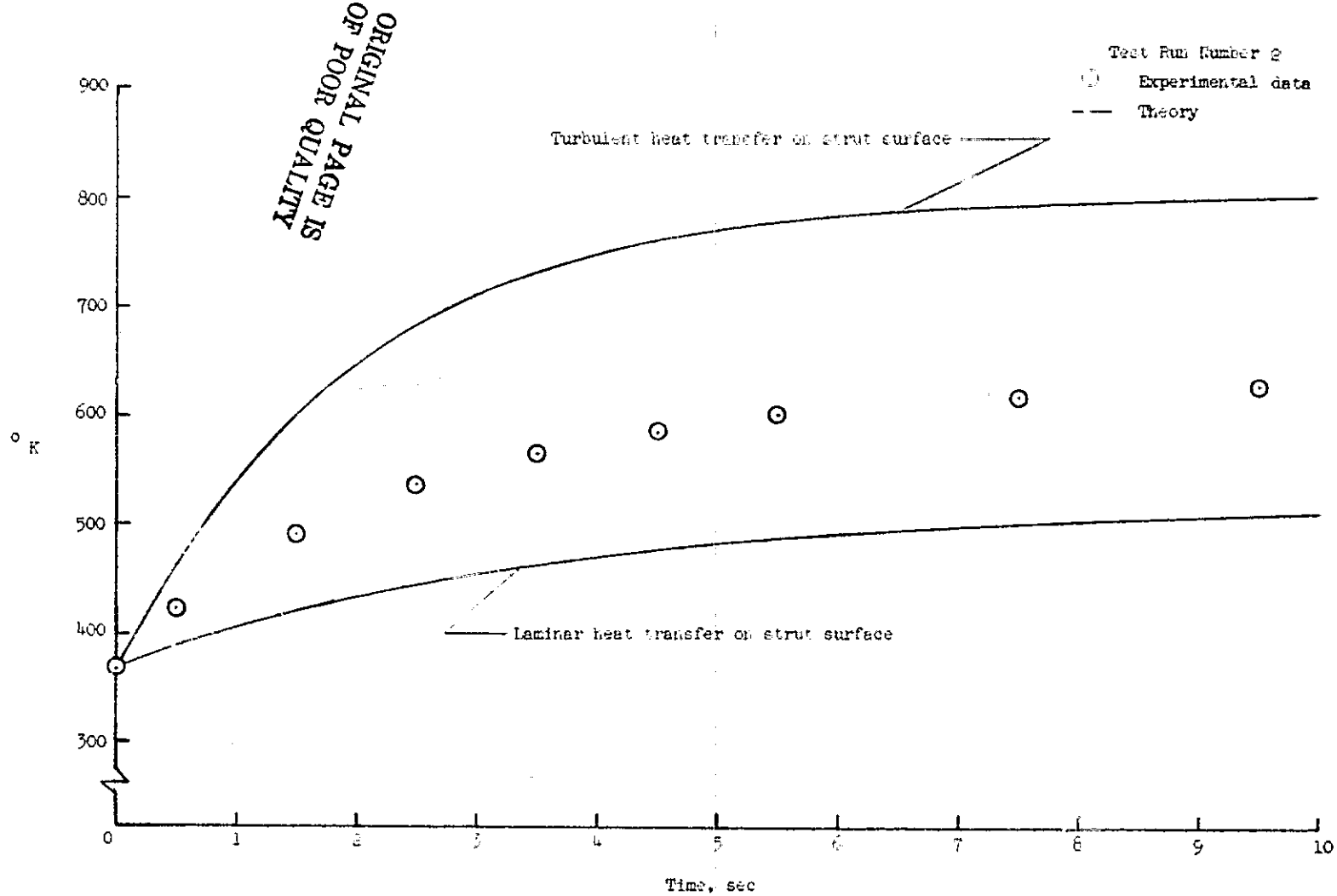

(c) Experimental and theoretical strut temperature versus time (laminar and turbulent boundary layers).

Figure 10. - Continued.

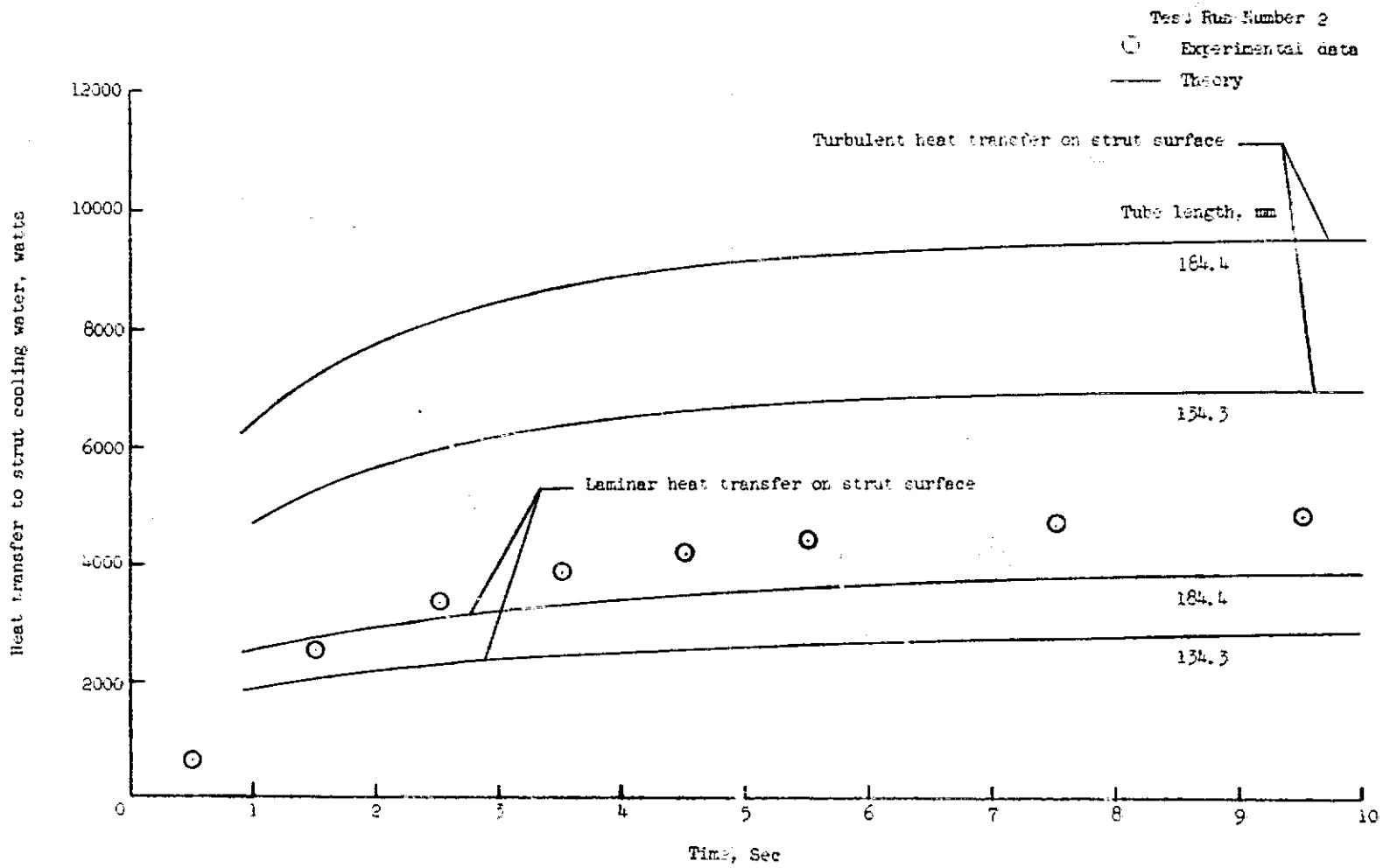

(c) Experimental and theoretical heat transfer rates to strut cooling water versus time (laminar and turbulent boundary layers).

Figure 10. - Concluded.

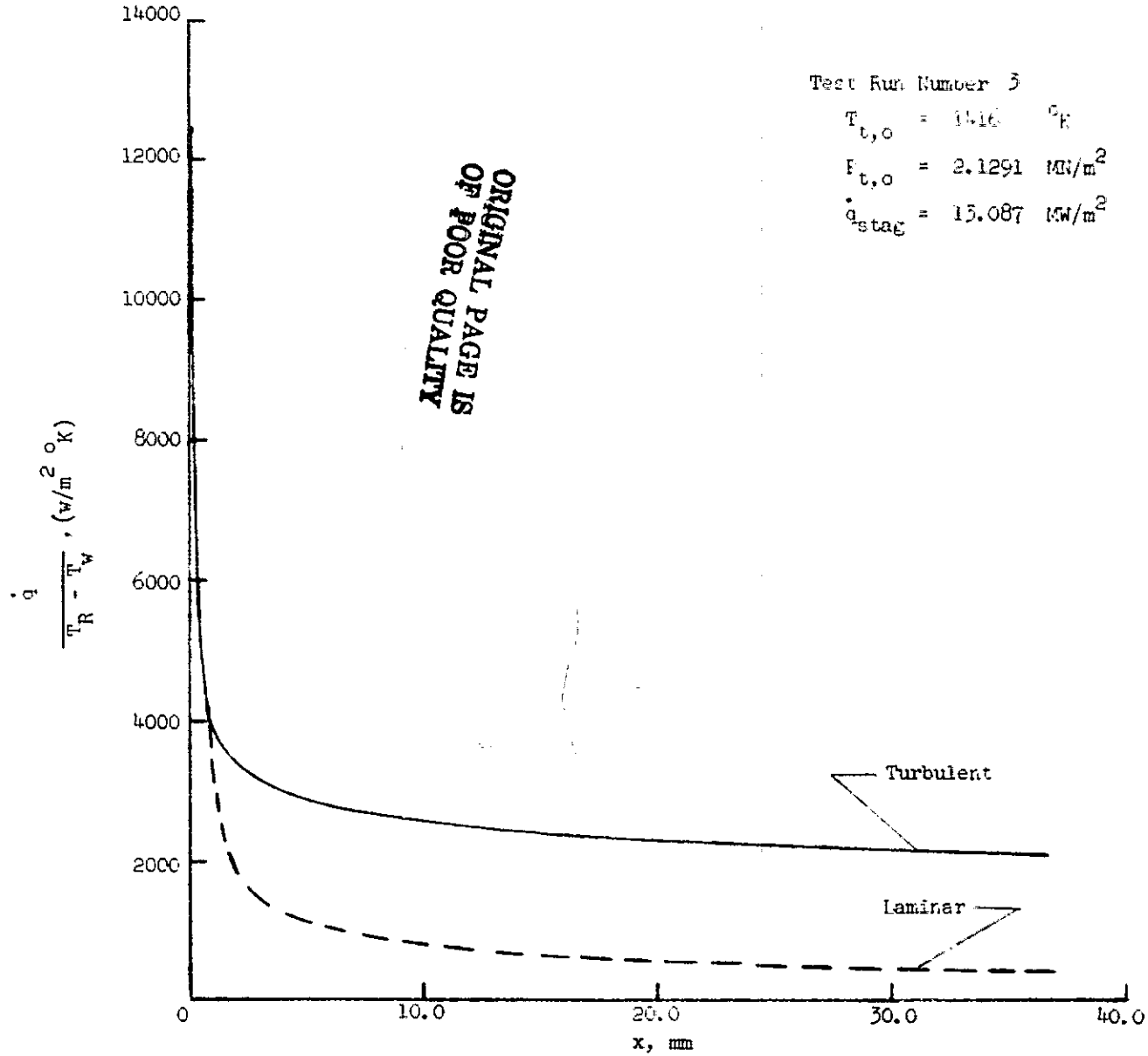

(a) Theoretical heat transfer coefficient along surface of strut (laminar and turbulent boundary layers).

Figure 11. - Experimental data and theoretical results for test run number 3.

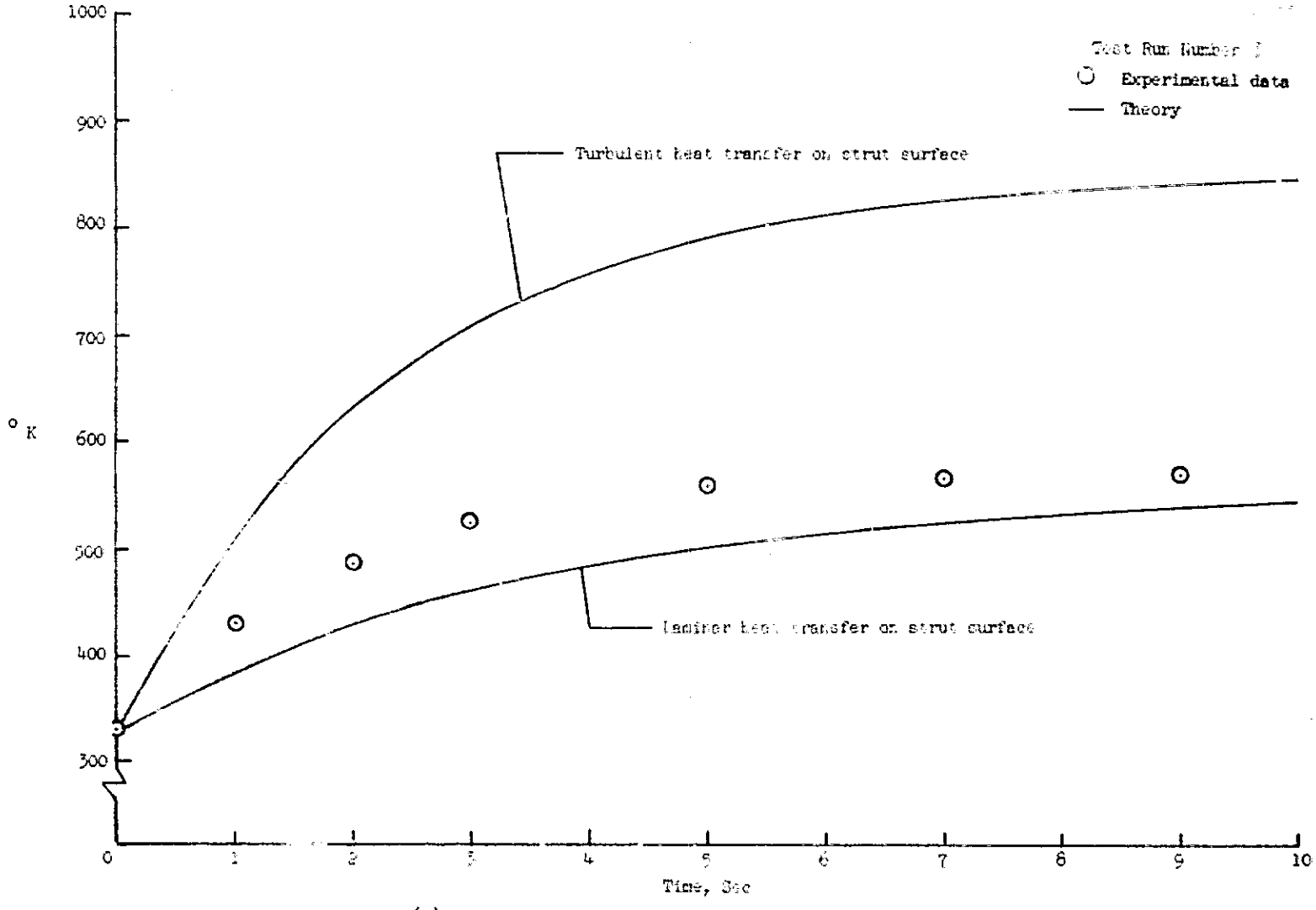

(c) Experimental and theoretical strut temperature versus time (laminar and turbulent boundary layers).

Figure 11. - Continued.

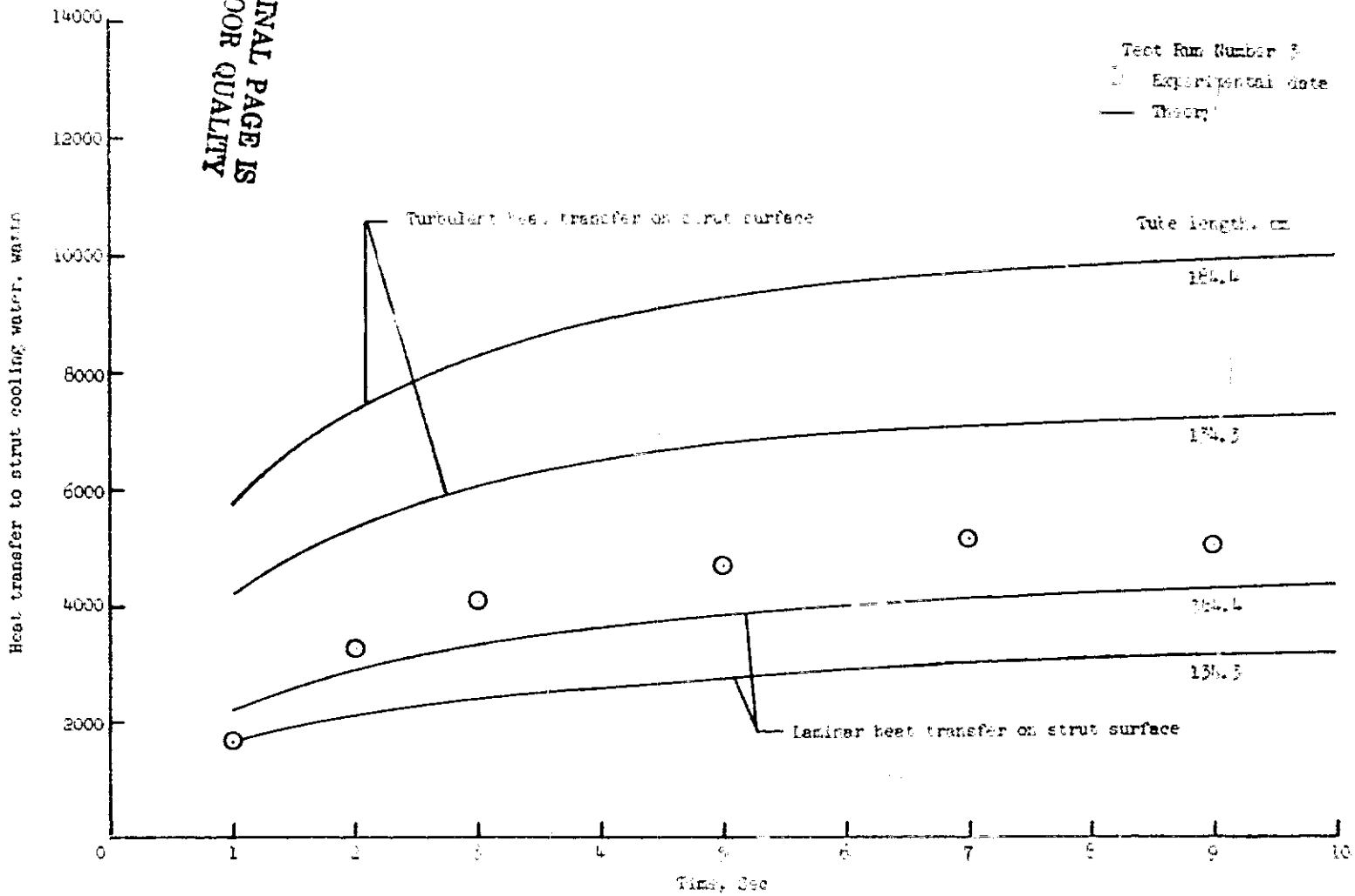

(c) Experimental and theoretical heat transfer rates to strut cooling water versus time (laminar and turbulent boundary layers).

Figure 11. - Concluded.

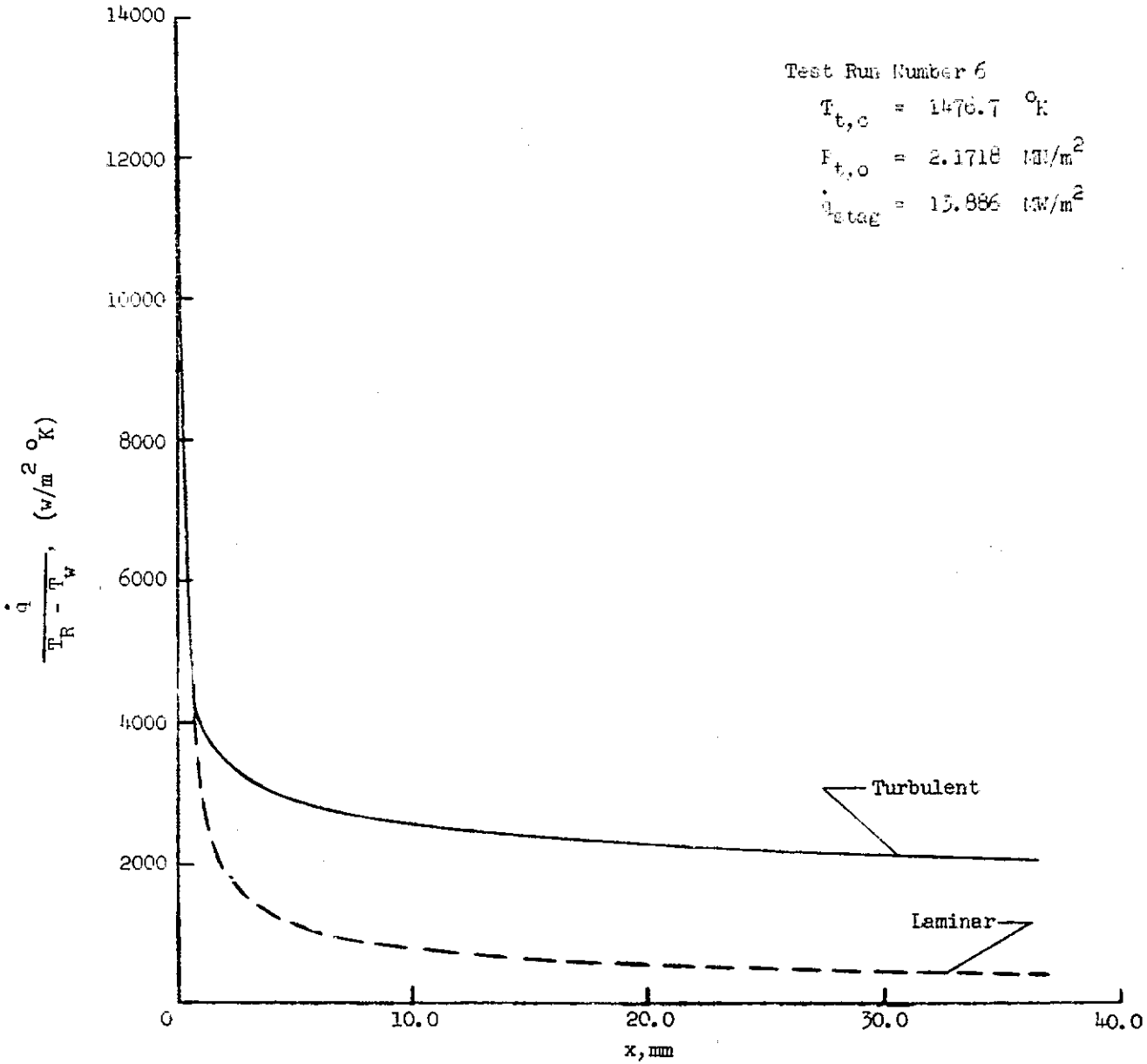

(a) Theoretical heat transfer coefficient along surface of strut (laminar and turbulent boundary layers).

Figure 12. - Experimental data and theoretical results for test run number 6.

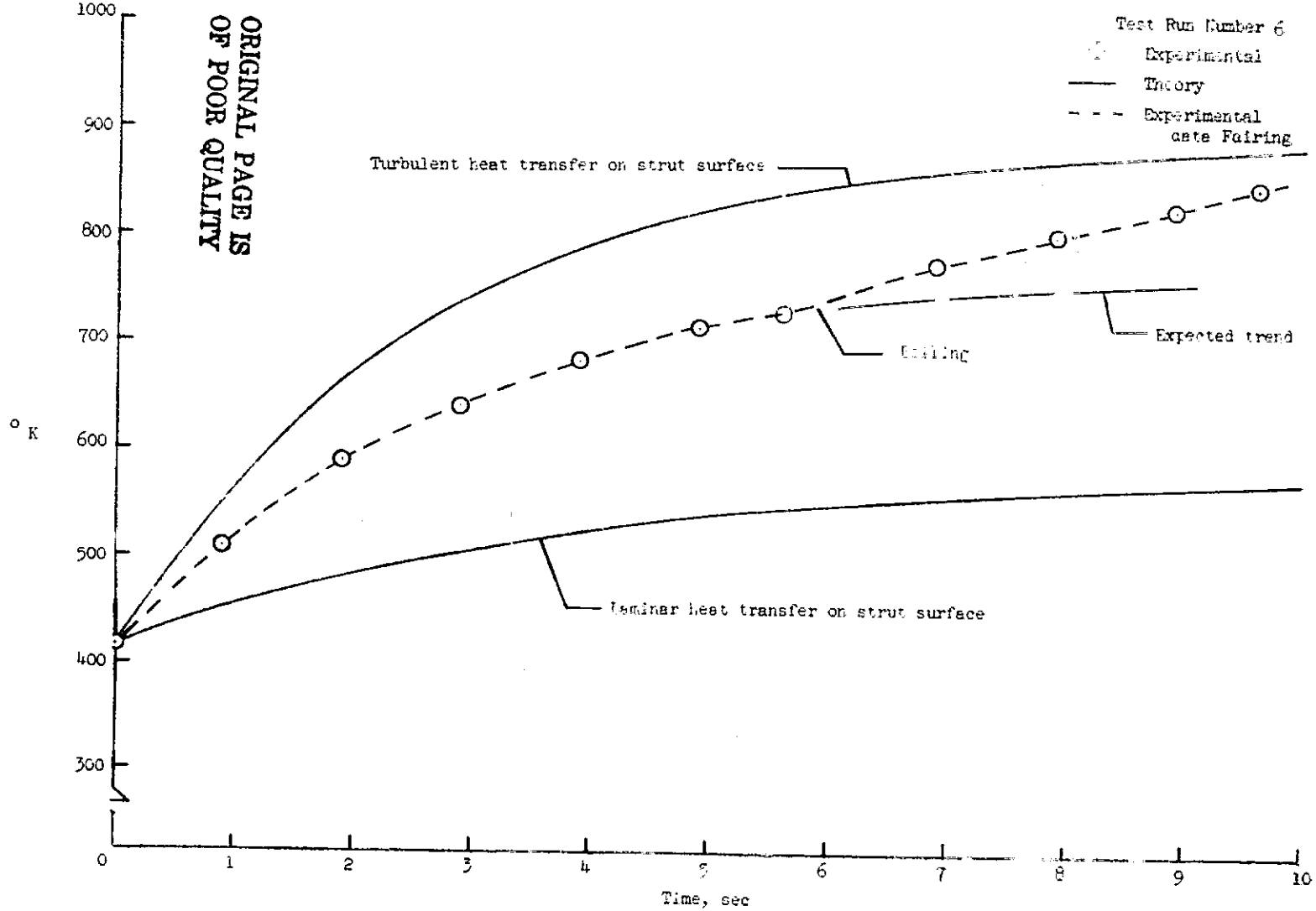

(c) Experimental and theoretical strut temperature versus time (laminar and turbulent boundary layers).

Figure 12. - Concluded.